
Momentum Stiefel Optimizer, with Applications to Suitably-Orthogonal Attention, and Optimal Transport

Lingkai Kong, Yuqing Wang, Molei Tao
 Georgia Institute of Technology
 {lkong75, ywang3398, mtao}@gatech.edu

Abstract

The problem of optimization on Stiefel manifold, i.e., minimizing functions of (not necessarily square) matrices that satisfy orthogonality constraints, has been extensively studied, partly due to rich machine learning applications. Yet, a new approach is proposed based on, for the first time, an interplay between thoughtfully designed continuous and discrete dynamics. It leads to a gradient-based optimizer with intrinsically added momentum. This method exactly preserves the manifold structure but does not require commonly used projection or retraction, and thus having low computational costs when compared to existing algorithms. Its generalization to adaptive learning rates is also demonstrated. Pleasant performances are observed in various practical tasks. For instance, we discover that placing orthogonal constraints on attention heads of trained-from-scratch Vision Transformer [1] could remarkably improve its performance, when our optimizer is used, and it is better that each head is made orthogonal within itself but not necessarily to other heads. This optimizer also makes the useful notion of Projection Robust Wasserstein Distance [2, 3] for high-dim. optimal transport even more effective.

1 Introduction

Matrices that satisfy orthogonal constraints are known to play important roles in numerous areas including machine learning. A wide range of studies have proven this both theoretically [4, 5] and experimentally – for example, orthogonality can boost the performances of a wide range of architectures, e.g., MLP [6], CNN and ResNet [7, 8], RNN [9–11], and Transformer [12]. The training of such models amounts to optimization under orthogonal constraints, whose applications to machine learning however are not restricted to just improving deep learning models. For example, such optimization helps construct optimal low-dim. projection of high-dim. data, which can be used for, e.g., robust and efficient approximation of Wasserstein distance [2, 3]. Therefore, this article will focus on this non-Euclidean / Riemannian optimization problem.

In fact, the set of matrices that contain orthogonal columns constitutes a Riemannian manifold known as Stiefel manifold. Given a pair of integers $n \geq m > 0$, it is defined as $\text{St}(n, m) := \{X \in \mathbb{R}^{n \times m} : X^\top X = I_{m \times m}\}$ (see Appendix A.3 for the $n = m$ special case which is almost $\text{SO}(n)$). Given a C^1 function $f : \text{St}(n, m) \rightarrow \mathbb{R}$ and gradient oracle, consider the smooth optimization problem

$$\min_{X \in \text{St}(n, m)} f(X), \quad \text{which is equivalent to} \quad \min_{X \in \mathbb{R}^{n \times m}, X^\top X = I_{m \times m}} f(X) \quad (1)$$

Due to the importance of this problem, a wide range of approaches have been proposed. Methods based on regularizers, which approximate the constraint (and hence the manifold structure), for example, have been popular in the machine learning literature [6, 8, 12, 13]. Meanwhile, efforts have been continuously made to construct algorithms that truly preserve the constraints (i.e. the manifold

structure), despite that challenges such as computational scalability and how to add momentum still remain; see two paragraphs below, and more discussions on existing milestones in Sec. 1.1.

Here is our strategy toward a good Stiefel optimizer: first, construct an optimizing dynamics in continuous time, described by a system of ODEs corresponding to damped mechanical systems on a constrained manifold; then, design a delicate time discretization of these ODEs, which gives optimization algorithms that precisely preserve the constraint and mimic the continuous dynamics.

Our approach has several pleasant properties: (1) The carefully designed ODE discretization retains exact preservation of the desired manifold structure, which allows the bypass of a need for traditional retraction techniques. Moreover, the discretization is stable in that it well preserves the structure even under low machine precision and numerous iterations, which are beneficial in machine learning contexts. (2) We have per-iteration computational complexity of $\mathcal{O}(nm^2)$, while other momentum methods that use retraction typically have at least $\mathcal{O}(n^2m)$ due to costly retraction (recall $n \geq$ or $\gg m$). Verifying the constraint by computing $X^\top X$ already costs $\mathcal{O}(nm^2)$. (3) Our approach intuitively generalizes to adaptive learning rate. We will ‘Stiefelize’ the popular Adam method [14] as a concrete example, although many other methods can be similarly generalized. (4) It gives a simple and geometrically natural way of adding momentum, which is a nontrivial challenge in manifold settings (e.g., [15–17]). Note these works also correspond to some of the remarkable results (e.g., [15–18]) that quantified the benefit of momentum in manifold optimization, under convexity. Although negative results in special cases also exist [19, 20], generally accepted is momentum can facilitate the training of deep learning models. However, tools are still lacking for quantitative analyses of nonconvex problems entailed by deep learning, even in Euclidean cases, let alone for applications considered here. Thus our demonstration in this regard will be empirical. (5) The same learning rate and momentum hyperparameters can be applied to both parameters with and without orthogonal constraints (Sec.3), unlike in previous milestones (e.g., [7]). This allows more efficient tuning, besides guaranteed convergence. It is a consequence of that both parameters are optimized under a unified variational framework and its structure preserving discretization. (6) Our algorithm is the first explicit retraction-free one that works for a range of Riemannian metrics, allowing great flexibility in choosing suitable geometry to optimize the performance for a specific problem.

Selected (due to space) experimental tests of our optimizer are: (1) We consider the simple problem of leading eigenvalues, which is yet practically important in data sciences, for systematically investigating algorithmic performances under different parameters. (2) We show the elegant idea of efficiently approximating optimal transport distance in high-dim. by seeking a good low-dim. projection [2, 3] can be made even more efficacious by our optimizer. (3) We note that Vision Transformer (ViT) can be further improved by imposing attention heads to be orthogonal. More precisely:

Consider training ViT from scratch. We discover that (1) requiring each head to be orthogonal in itself improves both training and testing the most. An important recent work [12] applied orthogonality to transformers and demonstrated improved performance in NLP tasks. It concatenates each of the W_i^Q , W_i^K , W_i^V matrices in attention across all heads, and apply orthogonal constraint to each of the three, via regularizer. This makes each head (approximately) orthogonal, not only within itself, but also to other heads. Orthogonal constraint is also applied to each weight matrix of feed-forward layers in their case. With our Stiefel optimizer which are not restricted to square matrices, we can now make each head exactly and only orthogonal within itself, which leads to further improvements at least in CV tasks. Meanwhile, (2) having orthogonality both in and across heads is found less effective than (1), but it is still better than requiring no orthogonality (i.e. vanilla ViT). No orthogonality on feed-forward layers was used in either (1) or (2). In addition, (3) to achieve these improvements, our Stiefel optimizer needs to be used; methods that do not have momentum or not exactly preserve structure (e.g., regularizer-based) are seen not fully exploiting the benefit of orthogonality.

1.1 More on related work

Orthogonality in deep learning Initialization: Orthogonal initialization is shown both theoretically and experimentally good for deep neural networks [4]. CNN: [6] uses regularizer to make weight matrices orthogonal when training fully connected neural network and CNN, and show both improved accuracy and robustness. [21] shows that posing orthogonality to CNN reduces overfitting. [13] experimentally compares several orthogonal regularizers on ResNet. RNN: Multiple results [9–11, 22, 23] show orthogonality helps plain RNN achieve long term memory and even out-perform advanced models such as LSTM. Transformer: Despite of its success, transformer is actually a recent

model, and to the best of our knowledge, the community just started applying orthogonal constraint to Transformer for NLP tasks [12]. Our work is the first to apply it to Vision Transformer [1].

Optimization algorithms Iterative orthogonal optimizers can be divided into two types: exact, and approximate structure preserving. Exact means each iteration is strictly on the manifold, i.e. exactly satisfying orthogonality. Otherwise it is approximate. Which one works better is theoretically still an open question, and likely task-dependent, but insightful empirical results exist.

For example, regularizer-based methods usually need more hyperparameter tuning, and the final result is likely sensitive to the extent of approximation (e.g., regularization strength [8]). They typically have low computational costs, but due to trajectory not exactly on the manifold, they may converge to (the neighborhood of) a local min. different from the one an exact algorithm converges to for multimodal problems. Similar observation was made for non-regularizer-based approximate method too; e.g., Vorontsov et al. [22] (will be discussed below) suggest at least in certain cases ‘hard’ constraint is better than ‘soft’. Meanwhile, we also note an interesting, non-regularizer-based recent result [24] that converges to the manifold despite of being approximate prior to convergence.

This paper considers exact orthogonality. For applications investigated here, empirical results suggest this is more beneficial (Sec.3.2 & Apdx.O). Existing approaches to exact preservation include:

Projection and/or retraction. Firstly, manifold optimization is a profound field (e.g., [15–17, 25–37]). General approaches for 1st-order (i.e. gradient based) optimization on (Riemannian) manifold typically involve two operations not present in Euclidean cases, projection and retraction. In each iteration of optimization, gradient needs to be a vector in tangent space (and momentum in cotangent space, if any), and the operation that maps nonintrinsic gradient to the tangent space is called projection. Then, the variable goes one step on manifold given the tangent vector, ideally via the exponential map, which however is often expensive or even not admitting a closed form computation, and approximation known as retraction is used. In the Stiefel manifold case, the exponential map has a well-known retraction approximation given by Cayley map, and Wen and Yin [38] proposed a gradient descent¹ method with smartly lowered computational cost of Cayley map, but this seminal result is hard to generalize to incorporate momentum or other metric (they essentially used canonical metric, i.e. Def.1 with $a = 1/2$). Li et al. [7] provided an iterative approximation for the computation of Cayley map and also obtained a momentum-accelerated optimizer, but it has $\mathcal{O}(n^2m)$ computational complexity per iteration due to the expensive Cayley map. These two methods will be referred to as {Momentumless Stiefel (S)GD} and {Projected Stiefel SGD/Adam} in this paper.

Matrix transformation based. It is possible to represent a Stiefel matrix by other matrices and optimize these matrices instead. A special case of $\text{SO}(n)$ was considered (e.g., [11, 23]) where $X = \text{expm}(A)$ or $X = \text{Cayley}(A)$ is used and then one optimizes skew symmetric A instead. However, this does not directly generalize to Stiefel, and the computational cost is high. Another work [22] uses SVD and retracts the singular values per step to maintain orthogonality, which is seminal but very expensive.

Structure preserving discretization of ODE. Exploiting the interplay between discrete and continuous dynamics has been attracting attention of the community. Here one first invents a differential equation (oftentimes an ODE system) that optimizes the objective function while preserving the constraints, and then designs numerical method for simulating the equation (a.k.a. time discretization or numerical integration). Our work falls into this kind. Tao and Ohsawa [39] used the same strategy and obtained momentum-accelerated optimizers for Lie groups, which include $\text{SO}(n)$, but their design is computationally costly to generalize to $\text{St}(n, m)$.

Table 1 compares the most relevant approaches. Rmk.5 in Appendix has more details on complexity.

We also mention the existence of useful algorithms for electronic structure calculations that are in fact Stiefel optimizers (e.g., [40–45]). However, to the best of our knowledge they are momentumless, based on retractions, sometimes not exactly manifold preserving, and sometimes even implicit. In addition, there are other interesting optimizers also based on discretizing damped mechanical systems but not via the splitting approach used here, e.g., [18, 46]; however they are again mostly implicit and therefore not always scalable to deep learning applications.

¹Their setting was deterministic, but an extension to use stochastic gradient descents is straightforward.

² \mathbf{u} stands for machine precision, which is a very small number

³This is the complexity under a fixed number of iterations for approximating Cayley map, which is their setup. $\mathcal{O}(n^2m(1 + \log(1/\mathbf{u})))$ instead if Cayley is computed to machine precision.

Optimizer	Complexity per iter	Pros and Cons
Stiefel SGD/Adam (Ours)	$\mathcal{O}(nm^2) + \mathcal{O}(m^3 \log \log (\frac{1}{\mathbf{u}}))^2$	<ul style="list-style-type: none"> ✓ structure preserving ✓ momentum and adaptive learning rate method ✓ single learning rate for ortho. and non-ortho. parameters ✓ a family of metrics
Projected Stiefel SGD/ Adam [7]	$\mathcal{O}(n^2m)^3$	<ul style="list-style-type: none"> ✓ momentum and adaptive learning rate method ✓ structure preserving ✗ single learning rate for ortho. and non-ortho. parameters
Momentumless Stiefel (S)GD [38]	$\mathcal{O}(nm^2)$	<ul style="list-style-type: none"> ✓ structure preserving ✗ generalize to other metric ✗ momentum
Regularizer	$\mathcal{O}(nm^2)$	<ul style="list-style-type: none"> ✓ fast in computing ✗ tasks that need strict orthogonality ✗ structure preserving ✗ sensitive to regularization strength

Table 1: Computational cost per iteration and a summary of pros and cons.

2 Derivation of the Optimizers and Their Properties

2.1 Preliminary

Recall Stiefel manifold $\text{St}(n, m) := \{X \in \mathbb{R}^{n \times m} : X^\top X = I_{m \times m}\}$ with $n \geq m$ contains matrices with orthonormal columns; ‘ (n, m) ’ will be omitted unless confusion arises. We will always consider Stiefel in this natural embedding and represent its elements as matrices, although the part outside the manifold in the embedded Euclidean space will never be used. We also represent elements in the tangent space and cotangent space by matrices using the following facts:

Proposition 1. The tangent space of St at X is $T_X \text{St} := \{\Delta \in \mathbb{R}^{n \times m} : X^\top \Delta + \Delta^\top X = 0\}$.

Proposition 2. Its tangent bundle is $T\text{St} := \{(X, \Delta) : X \in \text{St}, \Delta \in T_X \text{St}\}$.

Proposition 3. Its cotangent bundle is $T^*\text{St} := \{(X, P) : X \in \text{St}, P \in \mathbb{R}^{n \times m}, X^\top P + P^\top X = 0\}$.

Note our choice of coordinates is based the identity isomorphism $T_X^* \text{St} \cong T_X \text{St}$. See Appendix A.2. This paper focuses on a family of Riemannian metrics $g_X : T_X \text{St} \times T_X \text{St} \rightarrow \mathbb{R}$ on St defined as:

Definition 1 (canonical-type metric). For a fixed constant scalar $a < 1$, a metric for $\text{St}(n, m)$ with parameter a is defined as $g_X : T_X \text{St} \times T_X \text{St} \rightarrow \mathbb{R}$

$$g_X(\Delta_1, \Delta_2) = \text{Tr}(\Delta_1^\top (I - aXX^\top) \Delta_2), \quad \forall \Delta_1, \Delta_2 \in T_X \text{St} \quad (2)$$

Example. The following are two commonly used examples of the canonical-type metric (see [29]):

- When $a = 0$, $g_X(\Delta_1, \Delta_2) = \text{Tr}(\Delta_1^\top \Delta_2)$ which corresponds to the Euclidean metric.
- When $a = 1/2$, $g_X(\Delta_1, \Delta_2) = \text{Tr}(\Delta_1^\top (I - \frac{1}{2}XX^\top) \Delta_2)$, which is known as the canonical metric.

Notation. Denote Euclidean gradient in ambient vector space by $\frac{\partial f}{\partial X} := (\frac{\partial f}{\partial X_{ij}}(X))_{ij}$. Use \odot and \oslash for element-wise product and division, and $A^{\circ 2}$ and $A^{\circ 1/2}$ for element-wise square and root.

2.2 Optimization dynamics in continuous time

In Euclidean space, momentum has been long used as a way to accelerate gradient descent [47]. More recently, continuous time limit provided useful tools to complement the classical analyses for such optimizers (e.g., [48]), and then a variational formulation was established for a large family of momentum-accelerated methods [49]. This formulation provides a powerful and intrinsic way of generalizing momentum-based optimization to non-Euclidean settings. One demonstration is, for example, accelerated optimization on Lie groups [39]. Following the same line of thoughts, we define, for the sake of Stiefel optimization, a Lagrangian $L : T\text{St} \times \mathbb{R}_+ \rightarrow \mathbb{R}$ as follows

$$L(X, \dot{X}, t) = r(t) \left[\frac{1}{2} \text{Tr} \left(\dot{X}^\top (I - aXX^\top) \dot{X} \right) - f(X) \right]. \quad (3)$$

where $\dot{X} \in T_X \text{St}$ is the velocity, and $r : \mathbb{R}_+ \rightarrow \mathbb{R}_+$ is an increasing function that breaks the time invariance symmetry and thus introduces dissipation in the system.

With this Lagrangian, one could, in theory, consider a variational problem $\delta \int_0^T L(X(t), \dot{X}(t), t) dt = 0$ in the function space of $\{X(t) | 0 \leq t \leq T, [X(t), \dot{X}(t)] \in T\text{St}\}$. The corresponding stationarity

condition (known as Euler-Lagrange) yields an ODE that optimizes f in continuous time. However, to obtain concrete algorithms, we need the corresponding Euler-Lagrange ODE explicitly given in coordinates. In [39] this was achieved mainly by a tool known as reduction via Lie algebra, but this technique no longer applies to Stiefel manifold. In fact, Lie group $\text{SO}(n)$ is a special case of Stiefel manifold (when $n = m$), but when $n \neq m$, $\text{St}(n, m)$ is not a group and Lie algebra no longer exists.

Therefore, we treat this manifold optimization problem (1) instead as a constrained variational problem, using tools described in, e.g., [50]. More specifically, augment the Lagrangian to be

$$L(X, \dot{X}, \Lambda, t) = r(t) \left[\frac{1}{2} \text{Tr} \left(\dot{X}^\top (I - aXX^\top) \dot{X} \right) - f(X) \right] - \frac{1}{2} \text{Tr} (\Lambda^\top (X^\top X - I)) \quad (4)$$

where the symmetric matrix $\Lambda(t) \in \mathbb{R}^{m \times m}$ is a Lagrange multiplier⁴ for the constraints $X(t)^\top X(t) - I = 0$. Then, consider the variational problem $\delta \int_0^T L(X(t), \dot{X}(t), \Lambda(t), t) dt = 0$ in unconstrained function space $\{X(t), \Lambda(t) | 0 \leq t \leq T\}$. We have (proofs respectively in Apdx.C, D, E):

Theorem 1 (Optimization dynamics on St , with momentum). The variational principle gives ODE

$$\begin{cases} \dot{X} = Q \\ \dot{Q} = -\gamma Q - XQ^\top Q - \frac{3a}{2}(I - XX^\top)QQ^\top X - \frac{\partial f}{\partial X} + \frac{1+b}{2}XX^\top \frac{\partial f}{\partial X} + \frac{1-b}{2}X \frac{\partial f}{\partial X}^\top X \end{cases} \quad (5)$$

where $X(t), Q(t) \in \mathbb{R}^{n \times m}$ are state variable and its momentum, the scalar friction coefficient is $\gamma(t) := \dot{r}/r$, and $b := \frac{a}{a-1}$ is a metric dependent constant.

Theorem 2 (Constrained optimization with unconstrained dynamics). If the initial condition of (5) is in the cotangent bundle of Stiefel manifold, i.e. satisfying $X(0)^\top X(0) = I_{m \times m}$, $X(0)^\top Q(0) + Q(0)^\top X(0) = 0_{m \times m}$, then dynamics (5) automatically stay on the manifold (i.e. the cotangent bundle), i.e., for all $t \geq 0$, $X(t)^\top X(t) = I_{m \times m}$, $X(t)^\top Q(t) + Q(t)^\top X(t) = 0_{m \times m}$.

(5) is named ‘optimization dynamics’ because it is guaranteed to converge to a local minimizer:

Theorem 3 (Convergence to local minimum). For any isolated local minimum $X_* \in \text{St}$ of f , there exists a neighbourhood $U \subset T\text{St}$ of $(X_*, \mathbf{0})$ s.t., for any initial condition $(X_0, Q_0) \in U$, the solution of the system (5) satisfies $(X(t), Q(t)) \rightarrow (X_*, \mathbf{0})$ as $t \rightarrow \infty$.

Remark 1. For the sake of length, rate of convergence in specific situations (e.g., under geodesic convexity) will not be quantified, but it should be obtainable by combining tools in [18, 51].

Remark 2 (Choices of γ). Although monotonicity of r suffices for the convergence, choices of $\gamma = \dot{r}/r$ affect the convergence speed just like in Euclidean cases (e.g., [49, 51]). Popular choices include constant γ and $\gamma(t) = 3/t$, but methods proposed here work for all γ ’s (e.g., $\gamma = 3/t + ct^p$ for variance reduction [39]). However, for simplicity we will use constant γ from now on.

2.3 Structure-preserving discretization via variable decomposition and operator splitting

We now develop an integrator for (5) that is structure preserving⁵ and computationally efficient. Doing so is very difficult if one directly discretizes the time in (5). Instead, we first introduce a nontrivial decomposition of the tangent space, which then allows the design of a delicate numerical scheme. This section considers constant stepsize h , although it can actually differ between steps.

Let $Y = X^\top Q$ and $V = Q - XY$, and then the momentum can be decomposed as $Q = XY + V$. We then have $X \perp V$ in the sense that $X^\top V = 0$, and skew-symmetry of Y , i.e. $Y^\top = -Y$. Note Y is m -by- m (much smaller sized). See more explanation in Appendix B.1.

The structural constraints that X, Y, Z satisfy will help our time discretization, but prior to that is a nontrivial question: what ODEs should the new variables Y and Z follow, in order to maintain those constraints? Note the mn -dimensional Q dynamics will be replaced by $(m^2 + mn)$ -dimensional Y, V dynamics, and without constraints the latter is not uniquely obtainable. It turns out the following equivalent system will be structure-preserving (Thm.10) and amenable to good discretization:

$$\begin{aligned} \dot{X} &= XY + V, & \dot{Y} &= -\gamma Y - \frac{1-b}{2} \left(X^\top \frac{\partial f}{\partial X} - \frac{\partial f}{\partial X}^\top X \right), \\ \dot{V} &= -\gamma V + \frac{3a-2}{2} VY - XV^\top V - (I - XX^\top) \frac{\partial f}{\partial X}, \end{aligned} \quad (6)$$

⁴Note it differs from the seminal work of [38] as our setup (and hence the Lagrange multiplier) is dynamical.

⁵Throughout this paper, ‘structure preserving’ means exactly satisfying all constraints for all time. Staying exactly on Stiefel is also termed ‘feasible’ [24, 38], but we also have additional constraints due to momentum.

with initial condition satisfying $X(0)^\top X(0) = I, Y(0)^\top + Y(0) = 0, X(0)^\top V(0) = 0$.

Discretizing the time of eq.(6) is still nontrivial. The ODEs are highly nonlinear and admit no closed-form solutions. Moreover, although the continuous dynamics preserves the manifold structure when initialized as above, its discretization, in general, should not satisfy these constraints for all time. To overcome these difficulties, we adopt the operator splitting method based on the fact that a numerical discretization of the original ODE can be obtained as a composition of the (approximate) flow maps of the split ODEs (e.g., [52]). More precisely, in our splitting the vector field of (6) is viewed as a sum of three vector fields, each associated with one of the following ODEs:

$$\begin{cases} \dot{X} = XY \\ \dot{Y} = -\gamma Y \\ -\frac{1-b}{2} \left(X^\top \frac{\partial f}{\partial X} - \frac{\partial f}{\partial X}^\top X \right) \\ \dot{V} = 0 \end{cases} \quad (7) \quad \begin{cases} \dot{X} = 0 \\ \dot{Y} = 0 \\ \dot{V} = -\gamma V + \frac{3a-2}{2} VY \\ -(I - XX^\top) \frac{\partial f}{\partial X} \end{cases} \quad (8) \quad \begin{cases} \dot{X} = V \\ \dot{Y} = 0 \\ \dot{V} = -XV^\top V \end{cases} \quad (9)$$

A key reason for our specific split is that each split system admits structure-preserving solutions, both exact and approximate ones. Represent their exact solutions respectively by time- h evolution maps ϕ_1, ϕ_2, ϕ_3 , defined as $\phi_j : [X(t), Y(t), V(t)] \mapsto [X(t+h), Y(t+h), V(t+h)]$ for system j . Then

Theorem 4. ϕ_1, ϕ_2, ϕ_3 each maintains $X^\top X = I, Y^\top + Y = 0, X^\top V = 0$, i.e. each preserves the manifold structure. *Proof is in Appendix G.*

ϕ_1 and ϕ_3 do not admit analytical expressions. However, we can construct explicit structure-preserving approximations $\bar{\phi}_1$ and $\bar{\phi}_3$ that are also consistent in the sense that $\bar{\phi}_j : [X_0, Y_0, V_0] \mapsto [X_h, Y_h, V_h] = \phi_j([X_0, Y_0, V_0]) + \mathcal{O}(h^2), j = 1, 3$. They are defined as

$$\bar{\phi}_1 : \begin{cases} X_h = X_0 \expm(hY_h) \\ Y_h = \exp(-\gamma h)Y_0 \\ -\frac{(1-b)(1-\exp(-\gamma h))}{2\gamma} \left(X_0^\top \frac{\partial f}{\partial X_0} - \frac{\partial f}{\partial X_0}^\top X_0 \right) \\ V_h = V_0 \end{cases} \quad (10) \quad \bar{\phi}_3 : \begin{cases} X_\dagger = X_0 + hV_0X_0^\top X_0 \\ X_h = X_\dagger(X_\dagger^\top X_\dagger)^{-1/2} \\ Y_h = Y_0 \\ V_h = V_0 - hX_0V_0^\top V_0. \end{cases} \quad (11)$$

Theorem 5. The mappings (10) and (11) are structure preserving. *Proof is in Appendix H.*

ϕ_2 has exact solution (Appendix I.1) but a expm of size m -by- m matrix is included. If m is not too large, the usage of ϕ_2 suffices for a good algorithm; otherwise, the computational cost of expm can become prohibitive. In fact, Cayley transform (30) was commonly used as an approximation of matrix exponential. We however can further reduce this cost, and even simple discretization like forward Euler suffices:

Theorem 6. $\bar{\phi}_2$ given by $V_h = (1 - \gamma h)V_0 + \frac{3a-2}{2}hV_0Y_0 - h(I - X_0X_0^\top) \frac{\partial f}{\partial X}(X_0), X_h = X_0, Y_h = Y_0$ is structure preserving. *Proof is in Appendix I.2.*

We can now construct a method that integrates the new optimization dynamics (proof in Appendix J):

Theorem 7. One-step update given by $\bar{\phi}_1 \circ \bar{\phi}_2 \circ \bar{\phi}_3$, or any of the other 5 compositions with different orderings, is a structure-preserving, 1st-order (in h) numerical integrator of (6).

However, expm also appears in $\bar{\phi}_1$ and the same concern persists when m is large. Remarkable is, even if it gets replaced by a cheap, non-structure-preserving approximation in $\bar{\phi}_1$, we can still obtain a structure-preserving integrator in the end:

Theorem 8. Consider an approximation $\tilde{\phi}_1 = \bar{\phi}_1 + \mathcal{O}(h^2) = \phi_1 + \mathcal{O}(h^2)$. One-step update given by $\bar{\phi}_3 \circ \tilde{\phi}_1 \circ \bar{\phi}_2$, or any of the other 5 composition with different orderings, is a 1st-order (in h) numerical integrator of (6). Moreover, $\bar{\phi}_3 \circ \tilde{\phi}_1 \circ \bar{\phi}_2$ is also structure preserving. *Proof is in Appendix K.3*

Rather nontrivial is, other orderings may not give structure-preservation as $\bar{\phi}_1$ gets replaced by a cheap version $\tilde{\phi}_1$. The recovery of structure preservation in the above is partly due to the special design of $\bar{\phi}_3$. The update for X in $\bar{\phi}_3$ not only keeps it on the manifold but also is numerically stable to arithmetic errors due to finite machine precision. See more explanation in Appendix K.1.

Therefore, our default recommendation is to use $\bar{\phi}_3 \circ \tilde{\phi}_1 \circ \bar{\phi}_2$, where $\tilde{\phi}_1$ is $Y_h = (1 - \gamma h)Y_0 - \frac{1-b}{2}h \left(X_0^\top \frac{\partial f}{\partial X_0} - \frac{\partial f}{\partial X_0}^\top X_0 \right), X_h = X_0 + hY_h$. The result is concretely summarized in Algorithm 1. Note we also rescale parameters there to match the common notations in machine learning and discrete optimization: let the learning rate $\eta := \frac{1-\exp(-\gamma h)}{\gamma}h$, the momentum parameter $\mu := \exp(-\gamma h)$ $Z := Y / \frac{1-\exp(-\gamma h)}{\gamma}$ and $U := V / \frac{1-\exp(-\gamma h)}{\gamma}$. More information can be found in Appendix K.4.

If m is small, then $\bar{\phi}_1 \circ \phi_2 \circ \bar{\phi}_3$ (or any permutation) can also be used, although experimentally no clear advantage was observed (fig. 4). In fact, in this case, no matter whether expm (as in $\bar{\phi}_1$ and ϕ_2) or its Cayley approximation is used, its computational cost should not be a concern. This is because this operation is on an $m \times m$ matrix, not $n \times n$ as in existing approaches (e.g., [3, 7]).

Related but more important to discuss is the appearance of matrix inverse square root in the algorithm, because its computational cost should not be a concern either. On the one hand, it is again only for $m \times m$ matrices, not $n \times n$ which is often much larger. On the other hand, $(X_{\dagger}^{\top} X_{\dagger})^{-1/2}$ can be computed to machine precision rapidly using a quadratically convergent iterative method [53]; see Algorithm 3 in Appendix K.1 for details.

Algorithm 1: Momentum (S)GD on $\text{St}(n, m)$ (SGD: $\partial f / \partial X$ replaced by a stochastic estimator)

Hyperparameter: $\eta \in (0, +\infty)$, $\mu \in [0, 1)$, maximum number of iterations N

Initialization : X_0, U_0, Z_0 s.t. $X_0^{\top} X_0 = I$, $X_0^{\top} U_0 = 0$, $Z_0 + Z_0^{\top} = 0$

1 **for** $i = 0, \dots, N - 1$ **do**

2 Compute ‘gradients’: $f_i = \frac{1-b}{2} \left(X_i^{\top} \frac{\partial f}{\partial X}(X_i) - \frac{\partial f}{\partial X}^{\top}(X_i) X_i \right)$; $g_i = (I - X_i X_i^{\top}) \frac{\partial f}{\partial X}(X_i)$

3 Update $\bar{\phi}_2$: $U_{i+\frac{1}{2}} = \mu U_i - \frac{3a-2}{2} \eta U_i Z_i - g_i$

4 Update $\bar{\phi}_1$: $Z_{i+1} = \mu Z_i - f_i$; $X_{i+\frac{1}{2}} = X_i + \eta X_i Z_i$

5 Update ϕ_3 : $X_{\dagger} = X_{i+\frac{1}{2}} + \eta U_{i+\frac{1}{2}} X_{i+\frac{1}{2}}^{\top} X_{i+\frac{1}{2}}$; Compute $(X_{\dagger}^{\top} X_{\dagger})^{-\frac{1}{2}}$ using Algorithm 3;

$X_{i+1} = X_{\dagger} (X_{\dagger}^{\top} X_{\dagger})^{-\frac{1}{2}}$; $U_{i+1} = U_{i+\frac{1}{2}} - \eta X_{i+\frac{1}{2}} U_{i+\frac{1}{2}}^{\top} U_{i+\frac{1}{2}}$

6 **end**

7 **return** X_N

Remark 3. $\bar{\phi}_1 \circ \phi_2 \circ \bar{\phi}_3$ and other 5 compositions with different ordering each corresponds to a conformally symplectic integrator [39]. When $\gamma = 0$ they are all symplectic, and so is Alg.1.

2.4 An adaptive learning rate version

Tuning for the best learning rate can be labor intensive and computationally unaffordable, and sometimes SGD even performs worse than adaptive methods [54]. Thus, we now propose an adaptive version of our Stiefel optimizer. We will take Adam [55] as an example, which estimates the 1st and 2nd moments of gradients to obtain element-wise step sizes, or equivalently, a rescaling of gradient.

Our Stiefel SGD with momentum (Alg.1) could be interpreted as taking $\frac{1-b}{2} (X^{\top} \frac{\partial f}{\partial X} - \frac{\partial f}{\partial X}^{\top} X)$ and $(I - X(X^{\top} X)^{-1} X^{\top}) \frac{\partial f}{\partial X}$ as the ‘gradients’ in Y/Z and V/U direction. One of the main difficulties to extend Adam to the Stiefel setting is that the spaces where Y and V are located change with X and thus it’s challenging to remain on the tangent bundle. As a solution, we design an extra projection to ‘ V direction’ by $I - X X^{\top}$ for updating V while carefully adjust Y to maintain its skew-symmetry.

Combining all the above, we obtain the Adam-Stiefel optimizer. Denote $\hat{\phi}_1, \hat{\phi}_2, \hat{\phi}_3$ to be the modification of ϕ_1, ϕ_2, ϕ_3 in the Adam version (see detailed expressions in Appendix K.5. Then the integrator is defined as $\hat{\phi}_3 \circ \hat{\phi}_1 \circ \hat{\phi}_2$. The moments estimation is completed in $\hat{\phi}_2$ and $\hat{\phi}_1$ and the element-wise adaptive time stepping is included in $\hat{\phi}_2$ and $\hat{\phi}_3$. Additionally, $\hat{\phi}_3$ incorporates the extra projection of V that preserves the manifold structure. The overall method is shown in Algorithm 2.

Theorem 9 (Stiefel Adam is structure-preserving). The Adam version of the Stiefel optimizer $\hat{\phi}_3 \circ \hat{\phi}_1 \circ \hat{\phi}_2$ is structure-preserving. *Proof is in Appendix L.*

3 Experiments

This section demonstrates our Stiefel optimizers (both SGD and Adam) on Projection Robust Wasserstein Distance [2, 3] and trained-from-scratch Vision Transformer [1]. They will also be compared with advanced Stiefel optimizers in Table 1. An additional experiment on leading eigenvalue problem is deferred to Appendix O. Good performance is observed in all three cases.

Canonical metric (i.e. $a = 1/2$ in eq.2) is used in all experiments to show that the gained performance is due to the algorithmic innovation but not an extra tuned knob. One exception is the leading

Algorithm 2: Adam on Stiefel manifold $\text{St}(n, m)$

Hyperparameter: $\eta \in (0, +\infty)$, $\beta_1 \in [0, 1)$, $\beta_2 \in [0, 1)$, $0 < \epsilon \ll 1$, number of iterations N **Initialization:** X_0, V_0, Y_0, p_0, q_0 s.t. $X_0^\top X_0 = I$, $X_0^\top U_0 = 0$, $Z_0 + Z_0^\top = 0$, $p_0 = p_0^\top$ 1 **for** $i = 0, \dots, N - 1$ **do**2 Compute ‘gradients’: $f_i = \frac{1-b}{2} (X_i^\top \frac{\partial f}{\partial X}(X_i) - \frac{\partial f}{\partial X}(X_i)^\top X_i)$; $g_i = (I - X_i X_i^\top) \frac{\partial f}{\partial X}(X_i)$ 3 2nd-moment estimation: $p_{i+1} = \beta_2 p_i + (1 - \beta_2) f_i^{\circ 2}$; $q_{i+1} = \beta_2 q_i + (1 - \beta_2) g_i^{\circ 2}$ 4 Update $\hat{\phi}_2$: $U_{i+\frac{1}{2}} = \beta_1 U_i - \frac{3a-2}{2} \eta U_i Z_i - (1 - \beta_1) g_i$ 5 Update $\hat{\phi}_1$: $Z_{i+1} = \beta_1 Z_i - (1 - \beta_1) f_i$;

$$X_{i+\frac{1}{2}} = X_i + \eta \sqrt{1 - \beta_2^{i+1}} X_i \left(Z_{i+1} \circ (p_{i+\frac{1}{2}}^{\circ \frac{1}{2}} + \epsilon) \right)$$

6 Update $\hat{\phi}_3$: $\tilde{U} = \sqrt{1 - \beta_2^{i+1}} (I - X_{i+\frac{1}{2}} (X_{i+\frac{1}{2}}^\top X_{i+\frac{1}{2}})^{-1} X_{i+\frac{1}{2}}^\top) (U_{i+\frac{1}{2}} \circ (q_{i+\frac{1}{2}}^{\circ \frac{1}{2}} + \epsilon))$;

$$X_{\dagger} = X_{i+\frac{1}{2}} + \eta \tilde{U} X_{i+\frac{1}{2}}^\top X_{i+\frac{1}{2}}; X_{i+1} = X_{\dagger} (X_{\dagger}^\top X_{\dagger})^{-\frac{1}{2}}; U_{i+1} = U_{i+\frac{1}{2}} - \eta X_{i+\frac{1}{2}} \tilde{U}^\top U_{i+\frac{1}{2}}$$

7 **end**8 **return** X_N

eigenvalue problem, which is intended to provide a systematic investigation of performances; both canonical and Euclidean metrics are tested there. More experimental details are in Appendix N.

3.1 Projection Robust Wasserstein Distance

Projection Robust Wasserstein Distance (PRW) [2, 3] is a notion recently proposed to improve the robustness of standard Wasserstein metric, especially in high-dim settings. The idea is to simultaneously look for a best projection of high-dim data (given by x_i, y_j respectively with weights r_i, c_j) to low-dim and an entropic regularized optimal transport plan between projected data, i.e.

$$\max_{U \in \text{St}(d, k)} \min_{\pi \in \mathbb{R}_+^{n \times n}, \sum_j \pi_{ij} = r_i, \sum_i \pi_{ij} = c_j} \sum_{i=1}^n \sum_{j=1}^n \pi_{i,j} \|U^\top x_i - U^\top y_j\|^2 + \eta \langle \pi, \log(\pi) - 1_n 1_n^\top \rangle$$

This is a computationally challenging problem. Lin et al. [3] proposed an effective method based on alternations between a full Sinkhorn step [56], given the current projection, and an optimization step that improves the projection. In particular, they developed Riemmanian optimizer with projection and retraction (RGAS) and its adaptive learning rate version (RAGAS). We replace RGAS and RAGAS by our optimizer and others, and test on the hardest experiments in [3], namely MNIST and Shakespeare.

Results are in Fig.1 and our method is observed to find the largest value of PRW and thus the best projection among tested, which implies the best performance. Details of setup are in Appendix N.2.

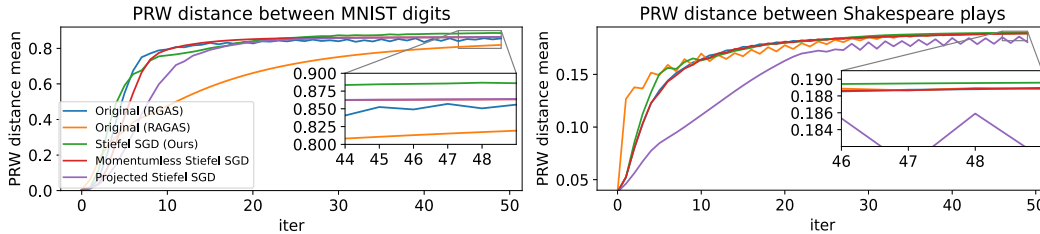


Figure 1: Projection Robust Wasserstein Distance (PRW) test on MNIST and Shakespeare plays. Data points are features extracted by some pre-trained model. The mean optimal transport value is taken among all digit or movie pairs and larger mean optimal transport value means more effective orthogonal projection. Our method makes PRW more effective by getting the best local minimum (largest optimal transport value) and fast convergence.

3.2 How orthogonality could be used to improve vanilla Vision Transformer (ViT)?

This section explores the possibility of making self-attention in Transformer models [57] orthogonal. The intuition is, if we interpret each attention head as a characterization of interactions between tokens, maybe linearly dependent interactions shouldn’t be double-counted for a more efficient and

ViT trained from scratch (6.3M parameters) test error (mean \pm std of 5 tests, in percentage)			
	Method	CIFAR 10	CIFAR 100
Orthogonality across heads	Stiefel SGD (ours, same as [39] in this case)	8.85 \pm 0.35	31.51 \pm 0.39
	Projected Stiefel SGD[7]	9.65 \pm 0.23	32.14 \pm 0.48
	Regularizer SGD	9.58 \pm 0.21	32.77 \pm 0.23
	Stiefel Adam (ours)	8.81 \pm 0.22	32.48 \pm 0.24
	Projected Stiefel Adam[7]	11.58 \pm 0.24	33.98 \pm 0.12
	Regularizer Adam	11.09 \pm 0.26	33.90 \pm 0.24
Orthogonality only within each head	Stiefel SGD (ours)	8.32 \pm 0.39	30.20 \pm 0.55
	Projected Stiefel SGD [7]	8.90 \pm 0.18	31.71 \pm 0.26
	Regularizer SGD	9.78 \pm 0.14	33.08 \pm 0.42
	Momentumless Stiefel SGD [38] \diamond	12.90 \pm 0.22	34.84 \pm 0.24
	Stiefel Adam (ours)	8.46 \pm 0.20	31.04 \pm 0.35
	Projected Stiefel Adam [7]	10.77 \pm 0.30	33.73 \pm 0.54
No constraints (baseline)	SGD	9.75 \pm 0.37	32.61 \pm 0.30
	Adam	9.52 \pm 0.32	33.15 \pm 0.50

Table 2: Orthogonal Vision Transformer (Stiefel-ViT) trained from scratch for CIFAR. For each of the 4 classes ($\{\text{across, only within}\} \times \{\text{SGD, Adam}\}$), blue is best within that class. Underlined is the best over all classes, and bold faced are methods from this paper.

\diamond : only tested for ‘within each head’ because it becomes ortho. SGD [39] with 0 momentum for ‘across head’.

robust characterization. In addition, there is unlikely just one way in which tokens relate to each other, and multiple heads handle different characterizations in parallel, so our second question is, should different heads also be orthogonal to each other?

To formulate precisely, we follow the notation of [57] and only review relevant parts: a Scaled Dot-Product multihead attention is given by $\text{MultiHead}(Q, K, V) = \text{Concat}(\text{head}_1, \dots, \text{head}_{n_{\text{head}}})W^O$, where $\text{head}_i = \text{Attention}(QW_i^Q, KW_i^K, VW_i^V)$, $\text{Attention}(\tilde{Q}, \tilde{K}, \tilde{V}) = \text{softmax}(\frac{\tilde{Q}\tilde{K}^\top}{\sqrt{d_k}})\tilde{V}$, matrices $W_i^Q \in \mathbb{R}^{d_{\text{model}} \times d_k}$, $W_i^K \in \mathbb{R}^{d_{\text{model}} \times d_k}$, $W_i^V \in \mathbb{R}^{d_{\text{model}} \times d_v}$ and $W^O \in \mathbb{R}^{n_{\text{head}}d_v \times d_{\text{model}}}$ correspond to trainable parameters. The three input matrices Q , K and V all have dimension $\text{sequence_length} \times d_{\text{model}}$. d_k and d_v are usually smaller than d_{model} .

For orthogonality only **within** head, we require W_i^Q, W_i^K are in $\text{St}(d_{\text{model}}, d_k)$. This needs $d_{\text{model}} \geq d_k$, which holds in most cases. For orthogonality **across** heads, we need $d_{\text{model}} \geq n_{\text{head}}d_k$, which is satisfied in many popular models, and we require $\text{Concat}(W_i^Q, i = 1 \dots, n_{\text{head}})$, $\text{Concat}(W_i^K, i = 1 \dots, n_{\text{head}})$ to be in $\text{St}(d_{\text{model}}, n_{\text{head}}d_k)$.

We test these two types of constraints on vanilla ViT [1], trained from scratch. Results summarized in Table 2 (and Figure 2 in Appendix N.3) show: (1) requiring each head to be orthogonal just within itself leads to the most significant improvement of performance; (2) additionally requiring heads to be orthogonal to each other will actually be less effective, although that is still better than requiring no orthogonality; (3) both of the 2 orthogonal constraint **require** our optimizer to outperform the non-constraint baseline. Otherwise negative effect may occur in certain cases; (4) momentum significantly helps train orthogonal ViT; (5) simply imposing orthogonal constraint (with our optimizer) makes ViT outperform some carefully designed models of the same size that are trained from scratch (Table A3 in [58]). Note models trained from scratch are very different from pre-trained ViT. To have some realistic expectation of the performance of trained-from-scratch ViT, recall, for example, an improved ViT, PVT-T [59], has 9.49% and 30.38% error on CIFAR 10 and CIFAR 100, using 12.8M parameters, and another improvement, DeiT-T [59], achieves 11.62% and 32.48% respectively with 5.3M parameters. Our model in Tab.2 (and Fig.2 in Appendix N.3) uses 6.3M parameters. More details about this experiment can be found in Appendix N.3.

Remark 4 (no additional hyperparameter needed for the Stiefel part). Our Stiefel-ViT model has both non-Euclidean and Euclidean parameters, the latter because we don’t impose orthogonality on feedforward layers and W_i^V . Our optimizer can use the same learning rate for both sets of parameters. This is because the optimizer is the time discretization of ODEs, and synchronous discretization is sufficient for convergence. This contrasts with other approaches such as projected Stiefel SGD/Adam [7], where learning rates for these two sets of parameters need to be adjusted separately and could differ by 40 times in some tasks. See Appendix N.1 for more discussion.

Acknowledgments and Disclosure of Funding

We thank Tomoki Ohsawa for insightful discussion. We are grateful for partial support by NSF DMS-1847802 (LK, YW and MT), NSF ECCS-1936776 (MT), and Cullen-Peck Scholar Award (LK, YW and MT).

References

- [1] Alexey Dosovitskiy, Lucas Beyer, Alexander Kolesnikov, Dirk Weissenborn, Xiaohua Zhai, Thomas Unterthiner, Mostafa Dehghani, Matthias Minderer, Georg Heigold, Sylvain Gelly, Jakob Uszkoreit, and Neil Houlsby. An image is worth 16x16 words: Transformers for image recognition at scale. *ICLR*, 2020.
- [2] François-Pierre Paty and Marco Cuturi. Subspace robust wasserstein distances. In *International conference on machine learning*, pages 5072–5081. PMLR, 2019.
- [3] Tianyi Lin, Chenyou Fan, Nhat Ho, Marco Cuturi, and Michael Jordan. Projection robust wasserstein distance and riemannian optimization. *Advances in neural information processing systems*, 33:9383–9397, 2020.
- [4] Andrew M Saxe, James L McClelland, and Surya Ganguli. Exact solutions to the nonlinear dynamics of learning in deep linear neural networks. *arXiv preprint arXiv:1312.6120*, 2013.
- [5] Lechao Xiao, Yasaman Bahri, Jascha Sohl-Dickstein, Samuel Schoenholz, and Jeffrey Pennington. Dynamical isometry and a mean field theory of cnns: How to train 10,000-layer vanilla convolutional neural networks. In *International Conference on Machine Learning*, pages 5393–5402. PMLR, 2018.
- [6] Moustapha Cisse, Piotr Bojanowski, Edouard Grave, Yann Dauphin, and Nicolas Usunier. Parseval networks: Improving robustness to adversarial examples. In *International Conference on Machine Learning*, pages 854–863. PMLR, 2017.
- [7] Jun Li, Fuxin Li, and Sinisa Todorovic. Efficient Riemannian optimization on the Stiefel manifold via the Cayley transform. *ICLR*, 2020.
- [8] Jiayun Wang, Yubei Chen, Rudrasis Chakraborty, and Stella X Yu. Orthogonal convolutional neural networks. In *Proceedings of the IEEE/CVF conference on computer vision and pattern recognition*, pages 11505–11515, 2020.
- [9] Martin Arjovsky, Amar Shah, and Yoshua Bengio. Unitary evolution recurrent neural networks. In *International Conference on Machine Learning*, pages 1120–1128. PMLR, 2016.
- [10] Scott Wisdom, Thomas Powers, John Hershey, Jonathan Le Roux, and Les Atlas. Full-capacity unitary recurrent neural networks. *Advances in neural information processing systems*, 29, 2016.
- [11] Kyle Helfrich, Devin Willmott, and Qiang Ye. Orthogonal recurrent neural networks with scaled cayley transform. In *International Conference on Machine Learning*, pages 1969–1978. PMLR, 2018.
- [12] Aston Zhang, Alvin Chan, Yi Tay, Jie Fu, Shuohang Wang, Shuai Zhang, Huajie Shao, Shuochao Yao, and Roy Ka-Wei Lee. On orthogonality constraints for transformers. In *Proceedings of the 59th Annual Meeting of the Association for Computational Linguistics and the 11th International Joint Conference on Natural Language Processing (Volume 2: Short Papers)*, pages 375–382, 2021.
- [13] Nitin Bansal, Xiaohan Chen, and Zhangyang Wang. Can we gain more from orthogonality regularizations in training deep networks? *Advances in Neural Information Processing Systems*, 31, 2018.
- [14] Diederik P Kingma and Jimmy Ba. Adam: A method for stochastic optimization. *ICLR*, 2015.
- [15] Hongyi Zhang and Suvrit Sra. An estimate sequence for geodesically convex optimization. In *Conference On Learning Theory*, pages 1703–1723. PMLR, 2018.
- [16] Kwangjun Ahn and Suvrit Sra. From nesterov’s estimate sequence to riemannian acceleration. In *Conference on Learning Theory*, pages 84–118. PMLR, 2020.

- [17] Foivos Alimisis, Antonio Orvieto, Gary Becigneul, and Aurelien Lucchi. Momentum improves optimization on riemannian manifolds. In *International Conference on Artificial Intelligence and Statistics*, pages 1351–1359. PMLR, 2021.
- [18] Valentin Duruisseaux and Melvin Leok. A variational formulation of accelerated optimization on riemannian manifolds. *arXiv preprint arXiv:2101.06552*, 2021.
- [19] Linus Hamilton and Ankur Moitra. No-go theorem for acceleration in the hyperbolic plane. *arXiv preprint arXiv:2101.05657*, 2021.
- [20] Christopher Criscitiello and Nicolas Boumal. Negative curvature obstructs acceleration for geodesically convex optimization, even with exact first-order oracles. *arXiv preprint arXiv:2111.13263*, 2021.
- [21] Pau Rodríguez, Jordi Gonzalez, Guillem Cucurull, Josep M Gonfaus, and Xavier Roca. Regularizing cnns with locally constrained decorrelations. *ICLR*, 2017.
- [22] Eugene Vorontsov, Chiheb Trabelsi, Samuel Kadoury, and Chris Pal. On orthogonality and learning recurrent networks with long term dependencies. In *International Conference on Machine Learning*, pages 3570–3578. PMLR, 2017.
- [23] Mario Lezcano-Casado and David Martinez-Rubio. Cheap orthogonal constraints in neural networks: A simple parametrization of the orthogonal and unitary group. In *International Conference on Machine Learning*, pages 3794–3803. PMLR, 2019.
- [24] Pierre Ablin and Gabriel Peyré. Fast and accurate optimization on the orthogonal manifold without retraction. In *International Conference on Artificial Intelligence and Statistics*, pages 5636–5657. PMLR, 2022.
- [25] Daniel Gabay. Minimizing a differentiable function over a differential manifold. *Journal of Optimization Theory and Applications*, 37(2):177–219, 1982.
- [26] Steven T Smith. Optimization techniques on riemannian manifolds. *Fields institute communications*, 3(3):113–135, 1994.
- [27] Alan Edelman, Tomás A Arias, and Steven T Smith. The geometry of algorithms with orthogonality constraints. *SIAM journal on Matrix Analysis and Applications*, 20(2):303–353, 1998.
- [28] P-A Absil, Robert Mahony, and Rodolphe Sepulchre. *Optimization algorithms on matrix manifolds*. Princeton University Press, 2009.
- [29] Hemant D Tagare. Notes on optimization on stiefel manifolds. *Yale University, New Haven*, 2011.
- [30] Sam Patterson and Yee Whye Teh. Stochastic gradient riemannian langevin dynamics on the probability simplex. In *Advances in neural information processing systems*, pages 3102–3110, 2013.
- [31] Hongyi Zhang and Suvrit Sra. First-order methods for geodesically convex optimization. In *Conference on Learning Theory*, pages 1617–1638, 2016.
- [32] Hongyi Zhang, Sashank J Reddi, and Suvrit Sra. Riemannian SVRG: Fast stochastic optimization on Riemannian manifolds. In *Advances in Neural Information Processing Systems*, pages 4592–4600, 2016.
- [33] Yuanyuan Liu, Fanhua Shang, James Cheng, Hong Cheng, and Licheng Jiao. Accelerated first-order methods for geodesically convex optimization on Riemannian manifolds. In *Advances in Neural Information Processing Systems*, pages 4868–4877, 2017.
- [34] Nicolas Boumal, Pierre-Antoine Absil, and Coralia Cartis. Global rates of convergence for nonconvex optimization on manifolds. *IMA Journal of Numerical Analysis*, 39(1):1–33, 2018.
- [35] Jiang Hu, Xin Liu, Zai-Wen Wen, and Ya-Xiang Yuan. A brief introduction to manifold optimization. *Journal of the Operations Research Society of China*, 8(2):199–248, 2020.
- [36] Jonathan W Siegel. Accelerated optimization with orthogonality constraints. *Journal of Computational Mathematics*, 39(2):207, 2021.
- [37] Guilherme França, Alessandro Barp, Mark Girolami, and Michael I Jordan. Optimization on manifolds: A symplectic approach. *arXiv preprint arXiv:2107.11231*, 2021.

- [38] Zaiwen Wen and Wotao Yin. A feasible method for optimization with orthogonality constraints. *Mathematical Programming*, 142(1):397–434, 2013.
- [39] Molei Tao and Tomoki Ohsawa. Variational optimization on lie groups, with examples of leading (generalized) eigenvalue problems. *International Conference on Artificial Intelligence and Statistics (AISTATS)*, pages 4269–4280, 2020.
- [40] Xin Zhang, Jinwei Zhu, Zaiwen Wen, and Aihui Zhou. Gradient type optimization methods for electronic structure calculations. *SIAM Journal on Scientific Computing*, 36(3):C265–C289, 2014.
- [41] Xiaoying Dai, Zhuang Liu, Liwei Zhang, and Aihui Zhou. A conjugate gradient method for electronic structure calculations. *SIAM Journal on Scientific Computing*, 39(6):A2702–A2740, 2017.
- [42] Bin Gao, Xin Liu, Xiaojun Chen, and Ya-xiang Yuan. A new first-order algorithmic framework for optimization problems with orthogonality constraints. *SIAM Journal on Optimization*, 28(1):302–332, 2018.
- [43] Bin Gao, Xin Liu, and Ya-xiang Yuan. Parallelizable algorithms for optimization problems with orthogonality constraints. *SIAM Journal on Scientific Computing*, 41(3):A1949–A1983, 2019.
- [44] Jiang Hu, Bo Jiang, Lin Lin, Zaiwen Wen, and Ya-xiang Yuan. Structured quasi-newton methods for optimization with orthogonality constraints. *SIAM Journal on Scientific Computing*, 41(4):A2239–A2269, 2019.
- [45] Xiaoying Dai, Qiao Wang, and Aihui Zhou. Gradient flow based kohn–sham density functional theory model. *Multiscale Modeling & Simulation*, 18(4):1621–1663, 2020.
- [46] Taeyoung Lee, Molei Tao, and Melvin Leok. Variational symplectic accelerated optimization on lie groups. *Conference on Decision and Control (CDC)*, 2021.
- [47] Yurii E Nesterov. A method for solving the convex programming problem with convergence rate $O(1/k^2)$. In *Dokl. akad. nauk Sssr*, volume 269, pages 543–547, 1983.
- [48] Weijie Su, Stephen Boyd, and Emmanuel Candes. A differential equation for modeling nesterov’s accelerated gradient method: theory and insights. *Advances in neural information processing systems*, 27, 2014.
- [49] Andre Wibisono, Ashia C Wilson, and Michael I Jordan. A variational perspective on accelerated methods in optimization. *Proceedings of the National Academy of Sciences*, 113(47):E7351–E7358, 2016.
- [50] Renyi Chen, Gongjie Li, and Molei Tao. Grit: A package for structure-preserving simulations of gravitationally interacting rigid bodies. *The Astrophysical Journal*, 919(1):50, 2021.
- [51] Ashia C Wilson, Ben Recht, and Michael I Jordan. A lyapunov analysis of accelerated methods in optimization. *Journal of Machine Learning Research*, 22(113):1–34, 2021.
- [52] Robert I McLachlan and G Reinout W Quispel. Splitting methods. *Acta Numerica*, 11:341–434, 2002.
- [53] Nicholas J Higham. Stable iterations for the matrix square root. *Numerical Algorithms*, 15(2):227–242, 1997.
- [54] Jingzhao Zhang, Sai Praneeth Karimireddy, Andreas Veit, Seungyeon Kim, Sashank Reddi, Sanjiv Kumar, and Suvrit Sra. Why are adaptive methods good for attention models? *Advances in Neural Information Processing Systems*, 33:15383–15393, 2020.
- [55] Diederik P Kingma and Jimmy Ba. Adam: A method for stochastic optimization. *ICLR*, 2015.
- [56] Marco Cuturi. Sinkhorn distances: Lightspeed computation of optimal transport. *Advances in neural information processing systems*, 26, 2013.
- [57] Ashish Vaswani, Noam Shazeer, Niki Parmar, Jakob Uszkoreit, Llion Jones, Aidan N Gomez, Łukasz Kaiser, and Illia Polosukhin. Attention is all you need. *Advances in neural information processing systems*, 30, 2017.
- [58] Zizhao Zhang, Han Zhang, Long Zhao, Ting Chen, Sercan Arik, and Tomas Pfister. Nested hierarchical transformer: Towards accurate, data-efficient and interpretable visual understanding. *AAAI*, 2022.

- [59] Wenhai Wang, Enze Xie, Xiang Li, Deng-Ping Fan, Kaitao Song, Ding Liang, Tong Lu, Ping Luo, and Ling Shao. Pyramid vision transformer: A versatile backbone for dense prediction without convolutions. In *Proceedings of the IEEE/CVF International Conference on Computer Vision*, pages 568–578, 2021.
- [60] Molei Tao. Explicit high-order symplectic integrators for charged particles in general electromagnetic fields. *Journal of Computational Physics*, 327:245–251, 2016.

Notation For simplicity, we denote $G := \frac{\partial f}{\partial X}$ when there is no confusion.

A Technical Remarks on Geometric Mechanics

A.1 Intuition of the cotangent bundle

If we require exact Stiefel manifold preservation for all time, i.e., $X(t)^\top X(t) = I$, a simple time differentiation gives a 2nd-order constraint $\dot{X}(t)^\top X(t) + X(t)^\top \dot{X}(t) = 0$ for $Q = \dot{X}$. This is why momentum Q has the additional structure $Q(t) \in T_{X(t)}^* \text{St}$.

A.2 What Exactly is Momentum?

Through this paper, we abused notation and called $Q := \dot{X}$ momentum, following the common practice of the community. It really should be called velocity instead, because although in canonical Euclidean spaces this doesn't make much a difference, for mechanical systems on manifolds they are not the same thing. For example, for our case, the geometrically intrinsic momentum variable should be given by Legendre transform

$$P := \frac{\partial L}{\partial \dot{X}} = r(I - aXX^\top)\dot{X} \quad (12)$$

instead, and velocity Q is in the tangent space while momentum P is in the cotangent space. In the paper we used the identity map for an isomorphism between the tangent and cotangent spaces, but if we'd like to make our variational formulation more elegant by viewing the kinetic energy as a natural pairing between the velocity and momentum variables, then the isomorphism should be given by the metric as in (12).

None of these affect the correctness or the efficacy of results in this paper. This discussion is just about terminology.

A.3 The special case of $\text{St}(n, n)$ and its relation with $O(n)$ and $\text{SO}(n)$

When $n \geq m$, $\text{St}(n, m) \cong O(n)/O(n-m)$; when $n > m$ strictly, we also have $\text{St}(n, m) \cong \text{SO}(n)/\text{SO}(n-m)$. However, in the special case of $n = m$, $\text{St}(n, n) \cong O(n)$ is not connected unlike the $n > m$ cases. Since our optimizer is based on the discretization of continuous dynamics, it cannot make jumps and thus just optimizes on a connected component of $\text{St}(n, m)$, which means for the special case of $n = m$, it is, to be precise, optimizing on $\text{SO}(n)$ but not $O(n)$, although a similar complication is nonexistent when $n > m$.

B About the Y, V decomposition

B.1 Derivation of their structural constraints

We first decompose the variable $Q \in T\text{St}$ by

$$Q = \begin{pmatrix} X & X^\perp \end{pmatrix} \begin{pmatrix} Y \\ Z \end{pmatrix} = XY + X^\perp Z, \quad (13)$$

where $X \in \text{St}(n, m)$, $Y \in \mathbb{R}^{m \times m}$, $Z \in \mathbb{R}^{(n-m) \times m}$; $X^\perp \in \mathbb{R}^{n \times (n-m)}$ is a matrix in the orthogonal complement of X , i.e., $X^\top \cdot X^\perp = \mathbf{0}_{m \times (n-m)}$. Let $V = X^\perp Z$. We have $X \perp V$ and

$$\begin{cases} Y = X^\top Q \\ V = Q - XY = (I - XX^\top)Q. \end{cases} \quad (14)$$

The above representation immediately implies Y is a skew-symmetric matrix since

$$X^\top Q + Q^\top X = 0 \Rightarrow Y^\top = -Y. \quad (15)$$

B.2 The advantage of the Y, V decomposition

The Y, V decomposition is near ‘orthogonal’ in the sense that $XY \perp V$ and it makes the metric separable. More precisely, consider our Y, V representation. $\forall \Delta_i \in T_X \text{St}, i = 1, 2$, if we denote $Y_{\Delta,i} = X^\top \Delta_i$ and $V_{\Delta,2} = (I - XX^\top) \Delta_i$, which means $\Delta_i = XY_{\Delta,i} + V_{\Delta,i}$, then the metric (2) can be rewritten as

$$\begin{aligned} g_X(\Delta_1, \Delta_2) &= \text{Tr}((XY_{\Delta,1} + V_{\Delta,1})^\top (I - aXX^\top)(XY_{\Delta,2} + V_{\Delta,2})) \\ &= (1 - a) \text{Tr}(Y_{\Delta,1}^\top Y_{\Delta,2}) + \text{Tr}(V_{\Delta,1}^\top V_{\Delta,2}). \end{aligned}$$

This means the metric of the tangent space is a linear combination of the metrics of Y and V -directions. Therefore, this gives an intuition why our continuous dynamics and numerical discretization in the following can handle the family of canonical-type metrics.

C Proof of Theorem 1

Proof. Given the Lagrangian

$$L(X, \dot{X}, \Lambda, t) = r(t) \left[\frac{1}{2} \text{Tr} \left(\dot{X}^\top (I - aXX^\top) \dot{X} \right) - f(X) \right] - \frac{1}{2} \text{Tr} (\Lambda^\top (X^\top X - I)), \quad (16)$$

Legendre transform gives momentum P as

$$P := \frac{\partial L}{\partial \dot{X}} = r(I - aXX^\top) \dot{X}.$$

One can equivalently switch the Hamiltonian picture, and the corresponding Hamiltonian is $H : T^* \text{St} \rightarrow \mathbb{R}$ with $H(X, P) := \text{Tr}(P^\top \dot{X}) - L$

$$H(X, P) = \frac{1}{2r} \text{Tr} [P^\top (I - bXX^\top) P] + rf(X) + \frac{1}{2} \text{Tr} [\Lambda^\top (X^\top X - I_{m \times m})] \quad (17)$$

where $b := \frac{a}{a-1}$ solves $(I - aXX^\top)(I - bXX^\top) = I$. Hence we get the following Hamilton’s equations

$$\begin{cases} \dot{X} = \frac{\partial H}{\partial P} = \frac{1}{r}(I - bXX^\top)P \\ \dot{P} = -\frac{\partial H}{\partial X} = \frac{b}{2r}(PP^\top X + XP^\top P) - r\frac{\partial f}{\partial X} - X\Lambda \end{cases} \quad (18)$$

Since $X^\top X \equiv I$, which gives $\dot{X}^\top X + X^\top \dot{X} = 0$. So we have $X^\top P + P^\top X = 0$. Take derivative to get $\dot{X}^\top P + X^\top \dot{P} + \dot{P}^\top X + P^\top \dot{X} = 0$, and use the condition that Λ is symmetric, we can solve Λ is

$$\Lambda = \frac{b+2}{2r} P^\top P - \frac{b}{2r} X^\top P P^\top X - \frac{r}{2} (X^\top G + G^\top X) \quad (19)$$

And (X, P) system becomes

$$\begin{cases} \dot{X} = \frac{\partial H}{\partial P} = \frac{1}{r}(I - bXX^\top)P \\ \dot{P} = -\frac{\partial H}{\partial X} = \frac{b}{2r} P P^\top X - \frac{1}{r} X P^\top P + \frac{b}{2r} X X^\top P P^\top X - rG + \frac{r}{2} (X X^\top G + X G^\top X) \end{cases} \quad (20)$$

By a coordinate change $Q := \frac{1}{r}(I - bXX^\top)P \in T_X \text{St}$ and define friction parameter $\gamma := \dot{r}/r$, Eq. (20) becomes

$$\begin{aligned} \dot{Q} &= -\frac{\dot{r}}{r^2}(I - bXX^\top)P + \frac{1}{r}(I - bXX^\top)\dot{P} - \frac{b}{r}\dot{X}X^\top P - \frac{b}{r}X\dot{X}^\top P \\ &= -\gamma Q - XQ^\top Q - \frac{3a}{2}(I - XX^\top)QQ^\top X - G + \frac{1+b}{2}XX^\top G + \frac{1-b}{2}XG^\top X \\ \begin{cases} \dot{X} = Q \\ \dot{Q} = -\gamma Q - XQ^\top Q - \frac{3a}{2}(I - XX^\top)QQ^\top X - G + \frac{1+b}{2}XX^\top G + \frac{1-b}{2}XG^\top X \end{cases} \quad (21) \end{aligned}$$

□

D Proof of Theorem 2

Proof. We can derive a new system of ODEs as

$$\begin{cases} \frac{d}{dt}(X^\top X) = X^\top Q + Q^\top X \\ \frac{d}{dt}(X^\top Q) = -\gamma X^\top Q - (I - X^\top X)Q^\top Q - \frac{3a}{2}X^\top(I - XX^\top)QQ^\top X \\ \quad - X^\top G + \frac{1+b}{2}X^\top XX^\top G + \frac{1-b}{2}X^\top XG^\top X \end{cases}$$

with viewing $X^\top G$ as a matrix function of t following Eq. (5). By the uniqueness and existence of ODE, we have that this system of ODE with variable $(X^\top X, X^\top Q)$ and initial condition $(I, 0)$ has the unique solution $X^\top X \equiv I, X^\top Q \equiv 0$. \square

E Proof of Theorem 3

Lemma 1 (First-order stationary point). If $X \in \text{St}$ s.t. $G - \frac{1+b}{2}XX^\top G - \frac{1-b}{2}XG^\top X = 0$, then $\forall \Delta \in T_X \text{St}$, we have $\text{Tr}(G^\top \Delta) = 0$, which means X is a first-order stationary point of f .

Proof. Left multiply both side of $G - \frac{1+b}{2}XX^\top G - \frac{1-b}{2}XG^\top X = 0$ by XX^\top , we have $XX^\top G = XG^\top X$, further we also have $G = XG^\top X$.

So we have

$$\begin{aligned} \text{Tr}(G^\top \Delta) &= \text{Tr}(X^\top G X^\top \Delta) \\ &= -\text{Tr}(X^\top G \Delta^\top X) \\ &= -\text{Tr}(\Delta^\top X X^\top G) \\ &= -\text{Tr}(\Delta^\top G) \end{aligned}$$

Thus we have $\text{Tr}(\Delta^\top G) = 0, \forall \Delta \in T_X \text{St}$, which means X is a 1-order stationary point of f . \square

Proof of Theorem 3. Let $t \rightarrow (X(t), Q(t))$ be a solution of Eq. (5). Define the ‘energy’ function $E : T\text{St} \rightarrow \mathbb{R}$ as

$$E(X, Q) := \frac{1}{2}\text{Tr}(Q^\top(I - aXX^\top)Q) + f(X) \quad (22)$$

This gives a Lyapunov function. So we have a neighbourhood U of $(X_*, 0)$ such that $E(X, Q) \geq f(X) \geq f(X_*)$ for any $(X, Q) \in U$. More over, since $X^\top Q + Q^\top X \equiv 0$, we have

$$\frac{dE}{dt}(X(t), Q(t)) = \text{Tr}(Q^\top(I - aXX^\top)\dot{Q}) - a\text{Tr}(Q^\top(\dot{X}X^\top)Q) + \text{Tr}\left(\frac{\partial f}{\partial X}^\top \dot{X}\right) \quad (23)$$

Using the fact that $X^\top Q + Q^\top X \equiv 0$, we have $\text{Tr}(Q^\top X Q^\top Q) = 0$ and $\text{Tr}(Q^\top X X^\top G) + \text{Tr}(Q^\top X G^\top X) = 0$, which gives

$$\frac{dE}{dt}(X(t), Q(t)) = -\gamma\text{Tr}(Q^\top(I - aXX^\top)Q) \leq 0 \quad (24)$$

Since we have r monotonely increasing, which means $\gamma = r'/r > 0, \forall t$. Then we have the energy is decreasing monotonically, implying that $Q = 0$ when converged. By lemma 1 that the limiting point for $X(t)$ is a first order stationary point, which is X_* since it is an isolated local minimum. \square

F XYV system is structure preserving

Theorem 10 (Constrained optimization with unconstrained dynamics). As long as the initial condition of (6) satisfies

$$X(0)^\top X(0) = I_{m \times m}, \quad Y(0) + Y(0)^\top = 0_{m \times m}, \quad X(0)^\top V(0) = 0_{m \times m},$$

then the dynamics automatically satisfies the same constraint, i.e.,

$$X(t)^\top X(t) = I_{m \times m}, \quad Y(t) + Y(t)^\top = 0_{m \times m}, \quad X(t)^\top V(t) = 0_{m \times m}, \quad (25)$$

Proof. By the uniqueness of solution of ODE, we know that the following ODE for $(X^\top X, Y^\top + Y, X^\top V)$, derived from Eq. (6), has a unique solution if view $V^\top V$ as an independent variable.

$$\begin{cases} \frac{d}{dt}(X^\top X) = X^\top XY + Y^\top X^\top X + X^\top V + V^\top X \\ \frac{d}{dt}(Y^\top + Y) = -\gamma(Y^\top + Y) \\ \frac{d}{dt}(X^\top V) = -\gamma X^\top V + Y X^\top V + \frac{3a-2}{2} X^\top V Y + (I - X^\top X) V^\top V \end{cases} \quad (26)$$

We can see that given initial condition $(X_0^\top X_0, Y_0^\top + Y_0, X_0^\top V_0) = (I, 0, 0)$, the unique solution is $(X^\top X, Y^\top + Y, X^\top V) \equiv (I, 0, 0)$. So we know that the constraint in Eq. (25) are preserved by continuous dynamics Eq. (6). \square

G Proof of Theorem 4

Proof. We assume the initial condition (X_0, Y_0, V_0) satisfies constraint (25).

For Eq. (7), we check $X^\top(t)X(t) \equiv 0$, $Y(t) + Y^\top(t) \equiv 0$ and $X^\top(t)V(t) = 0$.

$$\begin{aligned} \frac{d}{dt}(Y^\top + Y) &= \dot{Y}^\top + \dot{Y} \\ &= -\gamma(Y + Y^\top) \end{aligned}$$

with initial condition $Y_0 + Y_0^\top = 0$, we have $Y + Y^\top \equiv 0$

$$\begin{aligned} \frac{d}{dt}X^\top V &= \dot{X}^\top V + X^\top \dot{V} \\ &= Y^\top X V \end{aligned}$$

with initial condition $X_0^\top V_0 = 0$, we have $X^\top V \equiv 0$

$$\begin{aligned} \frac{d}{dt}X^\top X &= X^\top \dot{X} + \dot{X}^\top X \\ &= X^\top XY + X^\top V + Y^\top X^\top X + V^\top X \\ &= X^\top XY + Y^\top X^\top X \end{aligned}$$

Using the conclusion $Y + Y^\top \equiv 0$ that we have just proved and initial condition $X_0^\top X_0 = I$, we have $X^\top X \equiv 0$.

For Eq. (8), we need to check $X^\top(t)V(t) \equiv 0$. Since $X \equiv X_0$ and $Y \equiv Y_0$, we have

$$\begin{aligned} \frac{d}{dt}(X^\top V) &= X^\top \dot{V} \\ &= -\gamma X^\top V + \frac{3a-2}{2} X^\top V Y \end{aligned}$$

By uniqueness of the solution and initial condition $X_0^\top V_0 = 0$, we can see that $X(t)^\top V(t) \equiv 0$.

For Eq. (9), we need to check $\frac{d}{dt}(X^\top(t)X(t)) = 0$ and $\frac{d}{dt}(X^\top(t)V(t)) = 0$.

By the uniqueness of solution of ODE, we know that the following ODE for $(X^\top X, X^\top V, V^\top V)$, derived from Eq. (9), has a unique solution

$$\begin{cases} \frac{d}{dt}(X^\top X) = X^\top V + V^\top X \\ \frac{d}{dt}(X^\top V) = (I - X^\top X)V^\top V \\ \frac{d}{dt}(V^\top V) = -V^\top X V^\top V - V^\top V X^\top V \end{cases} \quad (27)$$

We can see that given initial condition $(X_0^\top X_0, X_0^\top V_0, V_0^\top V_0) = (I, 0, V_0^\top V_0)$, the unique solution is $(X^\top X, X^\top V, V^\top V) \equiv (I, 0, V_0^\top V_0)$. So we know that the constraint $X^\top X = I, X^\top V = 0$ are preserved by continuous dynamics Eq. (9).

□

H Proof of Theorem 5

Proof. **Eq. (10) is structure preserving.** We use the idea from [39]. Assume the initial value X_0, Y_0 and V_0 satisfies the constraint, i.e., $X_0^\top X_0 = I, Y_0 + Y_0^\top = 0$ and $X_0^\top V_0 = 0$. For the first step updating Y , due to the special form of the derivative of Y that is always skew-symmetric, we can tell that Y_h is also skew-symmetric and $Y_h + Y_h^\top = 0$. And the skew-symmetry of Y_h gives us that

$$\begin{aligned} X_h^\top X_h &= \text{expm}(hY_h^\top)X_0^\top X_0 \text{expm}(hY_h)^\top = 0 \\ X_h^\top V_h &= \text{expm}(hY_h^\top)X_0^\top V_0 = 0 \end{aligned}$$

so all 3 conditions in Eq. (25) are satisfied, meaning Eq. (10) is structure preserving.

Eq. (11) is structure preserving. First, we show that the discretization is a one order approximation of the exact solution. We get V_h and X_\dagger by forward Euler. And since X_0 and V_0 satisfies the constraint 25, we have

$$\begin{aligned} X_\dagger^\top X_\dagger &= (X_0 + hV_0)^\top (X_0 + hV_0) \\ &= (X_0^\top X_0 + hX_0^\top V_0 + hV_0^\top X_0 + h^2V_0^\top V_0) \\ &= I + h^2V_0^\top V_0 \end{aligned}$$

which means $X_h = X_\dagger + \mathcal{O}(h^2) = X_0 + hV_0 + \mathcal{O}(h^2)$, indeed a one order approximation of exact solution.

Next we show the numerical discretization is structure preserving. For constraint $X^\top V = 0$, we can check that

$$X_\dagger^\top V_h = X_0^\top V_0 + hX_0^\top X_0 V_0^\top V_0 - hX_0^\top X_0 V_0^\top V_0 - h^2V_0^\top X_0 V_0^\top V_0 = 0$$

which gives us $X_h^\top V_h = 0$. For restriction $X^\top X = I$, we have

$$X_h^\top X_h = (X_\dagger^\top X_\dagger)^{-\frac{1}{2}} X_\dagger^\top X_\dagger (X_\dagger^\top X_\dagger)^{-\frac{1}{2}} = I$$

□

I About ϕ_2 and $\bar{\phi}_2$

I.1 Exact solution for ϕ_2

The exact solution of ϕ_2 is given by $X(t+h) = X(t), Y(t+h) = Y(t)$, and with $M := \gamma I_{m \times m} - \frac{3a-2}{2}Y(t)$,

$$V(t+h) = V(t) \text{expm}(-Mh) - (I - X(t)X(t)^\top) \frac{\partial f}{\partial X}(X(t))M^{-1}(I - \text{expm}(-Mh)), \quad (28)$$

where $\text{expm}(\cdot)$ is matrix exponential.

I.2 Proof of Theorem 6

Proof. Given initial condition $X_0^\top X_0 = I$ and $X_0^\top V_0 = 0$, we check constraint $X_0^\top V_h = 0$.

$$X_0^\top V_h = (1 - \gamma h)X_0^\top V_0 + \frac{3a - 2}{2}hX_0^\top V_0 Y_0 - hX_0^\top (I - X_0 X_0^\top) \frac{\partial f}{\partial X}(X_0) = 0$$

□

J Proof of Theorem 7

Proof. The composition of structure-preserving maps is structure preserving. $\phi_1 \circ \phi_2 \circ \phi_3$ is a 1st-order integrator due to operator splitting theory [52], and its convergence order is kept after any ϕ_j gets replaced by $\hat{\phi}_j$ as long as the difference between $\hat{\phi}_j$ and ϕ_j is higher-order [60]. □

K Discussions on our numerical integrator

K.1 Benefits of the step $X_\dagger(X_\dagger^\top X_\dagger)^{-\frac{1}{2}}$

To remain the position X on the manifold, certain techniques that pull point back to manifold are used. For example, in [3, 7] for an n -by- m matrix X that is not on the manifold, they perform QR decomposition $X = QR$ and update the new X to be the first m columns of Q . However, the QR decomposition is not unique and such step does not have a closed form expression. More importantly, it cannot help design a structure-preserving scheme.

Instead, our algorithm has a similarly functioned step via the square root of the inverse matrix $X_h = X_\dagger(X_\dagger^\top X_\dagger)^{-1/2}$. In this case, it follows that $X_h^\top X_h = I$. This step is carefully designed from discretization of ODE ensuring the structure of X, Y, V is preserved at the same time. Through this update, we are able to obtain a structure-preserving method with a closed form expression (see the proof of Theorem 5 in Appendix H). Note that the square root of the inverse matrix can be iteratively solved with low computational cost (see Algorithm 3; [53]). It was proved to be quadratically convergent, which means only a couple of iterations are needed to reach machine precision, and only matrix multiplications are needed.

Algorithm 3: Algorithm for matrix root and matrix root inversion (Eq. (2.6) in [53])

Input: Symmetric m -by- m matrix A , tol

Initialization : $Y_0 = A, Z_0 = I_{m \times m}, k = 0$

```

1 while  $\|Y_k^2 - A\| \geq tol$  do
2    $Y_{k+1} = \frac{1}{2}Y_k(3I - Z_k Y_k)$ 
3    $Z_{k+1} = \frac{1}{2}(3I - Z_k Y_k)Z_k$ 
4    $k \leftarrow k + 1$ 
5 end
6 return  $Y_k \approx A^{\frac{1}{2}}$  and  $Z_k \approx A^{-\frac{1}{2}}$ 

```

Another benefit of this step is that it is more stable to the truncation error produced by finite machine precision (which can become a significant issue if the model is trained in single accuracy on consumer graphic cards or even quantized). Although $X_\dagger^\top X_\dagger$ follows the expression

$$\begin{aligned} X_\dagger^\top X_\dagger &= (X_0 + hV_0)^\top (X_0 + hV_0) \\ &= (X_0^\top X_0 + hX_0^\top V_0 + hV_0^\top X_0 + h^2V_0^\top V_0) \\ &= I + h^2V_0^\top V_0, \end{aligned}$$

the stability of $X_\dagger(X_\dagger^\top X_\dagger)^{-1/2}$ is much better than $X_\dagger(I + h^2V_0^\top V_0)^{-1/2}$. Particularly, when $n = m$, it is an identical map if there is no machine error.

K.2 Simplification of matrix exponential

There are two steps in the discretizations (28) and (10) that use the matrix exponential of $m \times m$ matrices. Similar matrix exponential is also shown in [7, 38] but with matrices of much larger size

$n \times n$ (note $n > m$). We introduce two ways of simplifying the computation of the matrix exponential. First, note that Cayley transform is a 2nd-order structure-preserving approximation of the matrix exponential, defined as follows

$$\text{Cayley}(hY) = (I - hY/2)^{-1}(I + hY/2) = \exp(hY) + \mathcal{O}(h^3). \quad (29)$$

By applying the Cayley transform, the computation is reduced to an inversion of matrix and matrix multiplication while it still keeps the variable on the manifold.

Additionally, we can use the first-order forward Euler to discretize the ODEs for the two steps, which is also the first-order truncation of the matrix exponential. In this case, the X update in scheme (10) is just $X_h = X_0 + hY_h$ and is no longer structure-preserving but structure-preserving property of the overall algorithm is not affected (see Thm. 8).

For scheme (28), its Cayley map approximation is structure preserving and defined as follows

$$V_h = V_0 \text{Cayley}(-\gamma hI + \frac{3a-2}{2}hV_0Y_0) - \frac{1 - \exp(-\gamma h)}{\gamma}(I - X_0X_0^\top) \frac{\partial f}{\partial X_0}. \quad (30)$$

Note the variable V will still satisfy the constraint (25) even if we change the update of V to forward Euler

$$V_h = V_0 - \gamma hV_0 + \frac{3a-2}{2}hV_0Y_0 - \frac{1 - \exp(-\gamma h)}{\gamma}(I - X_0X_0^\top) \frac{\partial f}{\partial X_0}. \quad (31)$$

In fact, the above two ways and the original matrix exponential share the same complexity per iteration. Also, we do not find any significant difference in the convergence in numerical experiments (Appendix O). Hence we will always use forward Euler as default, which has the lowest computational cost.

K.3 Proof of Theorem 8

Proof. The composition of $\bar{\phi}_1, \bar{\phi}_2, \bar{\phi}_3$ in any order will give a structure preserving scheme, because in Sec. H we proved that each of them is structure preserving.

When we apply it in specific order $\bar{\phi}_3 \circ \bar{\phi}_1 \circ \bar{\phi}_2$, we prove when $X^\top X = I$ is no longer preserved by $\bar{\phi}_2$, the assembled scheme is still structure preserving. We only need to prove that $[X_h, Y_h, V_h] = \bar{\phi}_3(x_0, Y_0, V_0)$ satisfies the following: when initial condition satisfies $Y_0^\top + Y_0 = 0$ and $X_0^\top V_0 = 0$, we have $X_h^\top X_h = I$, $Y_h^\top + Y_h = 0$ and $X_h^\top V_h = 0$.

Since we have the step $X_h = X_\dagger(X_\dagger^\top X_\dagger)^{-1/2}$, we have $X_h^\top X_h = I$. Y is not updating so $Y_h + Y_h^\top = 0$.

$$X_\dagger^\top V_h = X_0^\top V_0 - hX_0^\top X_0 V_0^\top V_0 + hX_0^\top X_0 V_0^\top V_0 - h^2 X_0^\top X_0 V_0^\top X_0 V_0^\top V_0 = 0$$

As a result, $X_h^\top V_h = (X_\dagger^\top X_\dagger)^{-1/2} X_\dagger^\top V_h = 0$

□

K.4 The integrator in rescaled coordinates used in Algorithm 1

$$\bar{\phi}_1 : \begin{cases} X_\eta = X_0 + \eta Z_h \\ Z_\eta = \mu Z_0 - \frac{1-b}{2} \left(X_0^\top \frac{\partial f}{\partial X_0} - \frac{\partial f}{\partial X_0}^\top X_0 \right) \\ U_\eta = U_0 \end{cases} \quad \bar{\phi}_2 : \begin{cases} X_\eta = X_0 \\ Z_\eta = Z_0 \\ U_\eta = \mu U_0 + \frac{3a-2}{2} \eta U_0 Z_0 \\ \quad - (I - X_0 X_0^\top) \frac{\partial f}{\partial X_0}, \end{cases}$$

$$\bar{\phi}_3 : \begin{cases} X_\dagger = X_0 + \eta U_0 X_0^\top X_0 \\ X_\eta = X_\dagger (X_\dagger^\top X_\dagger)^{-1/2} \\ Z_\eta = Z_0 \\ U_\eta = U_0 - \eta X_0 U_0^\top U_0 \end{cases}$$

K.5 The integrator in rescaled coordinates used in Algorithm 2

$$\begin{aligned}
\text{'gradient' and 2-order momentum : } & \begin{cases} f_i = \frac{1-b}{2} \left(X_i^\top \frac{\partial f}{\partial X}(X_i) - \frac{\partial f}{\partial X}(X_i)^\top X_i \right) \\ g_i = (I - X_i X_i^\top) \frac{\partial f}{\partial X}(X_i) \\ p_{i+1} = \beta_2 p_i + (1 - \beta_2) f_i^{\circ 2} \\ q_{i+1} = \beta_2 q_i + (1 - \beta_2) g_i^{\circ 2} \end{cases} \\
\hat{\phi}_1 : & \begin{cases} X_{i+1} = X_i + \eta \sqrt{1 - \beta_2^{i+1}} Z_{i+1} \circ (p_{i+1}^{\circ 1/2} + \epsilon) \\ Z_{i+1} = \beta_1 Z_i - (1 - \beta_1) f_i \\ U_{i+1} = U_i \end{cases} \quad \hat{\phi}_2 : \begin{cases} X_{i+1} = X_i \\ Z_{i+1} = Z_i \\ U_{i+1} = \beta_1 U_i - \frac{3a-2}{2} \eta U_i Z_i - (1 - \beta_1) g_i \end{cases} \\
\hat{\phi}_3 : & \begin{cases} \tilde{U} = \sqrt{1 - \beta_2^{i+1}} (I - X_i (X_i^\top X_i)^{-1} X_i^\top) (U_i \circ (q_{i+1}^{\circ 1/2} + \epsilon)) \\ X_\dagger = X_i + \eta \tilde{U} X_i^\top X_i \\ X_{i+1} = X_\dagger (X_\dagger^\top X_\dagger)^{-1/2} \\ Z_{i+1} = Z_i \\ U_{i+1} = U_i - \eta X_i \tilde{U}^\top U_i \end{cases}
\end{aligned}$$

L Proof of Theorem 9

Proof. We will use the same notation as in algorithm 2. Assume $X_i^\top X_i = I$, $Y_i^\top + Y_i = 0$, $X_i^\top V_i = 0$, $p_i = p_i^\top$. Our initialization satisfies these conditions. We prove that these conditions are satisfied after mapped by $\hat{\phi}_3 \circ \hat{\phi}_1 \circ \hat{\phi}_2$ in the following. **Step 1:** Due to the skew-symmetry of f_i , we have p_{i+1} is symmetric.

Step 2: $X_i, Z_i, U_{i+\frac{1}{2}} := \hat{\phi}_2(X_i, Z_i, U_i)$, where $U_{i+\frac{1}{2}} = \beta_1 U_i - \frac{3a-2}{2} \eta U_i Z_i - (1 - \beta_1) g_i$. Since $X_i^\top U_i = 0$ and $X_i^\top g_i = 0$, we can check

$$X_i^\top U_{i+\frac{1}{2}} = \beta_1 X_i^\top U_i - \frac{3a-2}{2} \eta X_i^\top U_i Z_i - (1 - \beta_1) X_i^\top g_i = 0$$

Step 3: $X_{i+\frac{1}{2}}, Z_{i+1}, U_{i+\frac{1}{2}} := \hat{\phi}_1(X_i, Z_i, U_{i+\frac{1}{2}})$, where $Z_{i+1} = \beta_1 Z_i - (1 - \beta_1) f_i$ and $X_{i+\frac{1}{2}} = X_i + \eta \sqrt{1 - \beta_2^{i+1}} X_i (Z_{i+1} \circ (p_{i+1}^{\circ \frac{1}{2}} + \epsilon))$.

Since we have $X_i^\top U_{i+\frac{1}{2}} = 0$ We can have directly $X_{i+\frac{1}{2}}^\top U_{i+\frac{1}{2}} = 0$. And due to f_i is symmetric, Z_{i+1} is still skew-symmetric. Note that $X_{i+\frac{1}{2}}^\top X_{i+\frac{1}{2}} = I$ no longer stands now but it satisfied until the algorithm finishes.

Step 4 $X_{i+1}, Z_{i+1}, U_{i+1} := \hat{\phi}_3(X_{i+\frac{1}{2}}, Z_{i+1}, U_{i+\frac{1}{2}})$. First we can see from $X_{i+1} = X_\dagger (X_\dagger^\top X_\dagger)^{-\frac{1}{2}}$ that $X_{i+1}^\top X_{i+1} = I$ as long as $X_\dagger = X_{i+\frac{1}{2}} + \eta \tilde{U} X_{i+\frac{1}{2}}^\top X_{i+\frac{1}{2}}$ is full rank, which is always true since X_i is full rank and η is small.

Since we have $X_{i+\frac{1}{2}}^\top \tilde{U} = 0$ by the special form of matrix $I - X_{i+\frac{1}{2}} (X_{i+\frac{1}{2}}^\top X_{i+\frac{1}{2}})^{-1} X_{i+\frac{1}{2}}^\top$

$$X_\dagger^\top U_{i+\frac{1}{2}} = \eta X_{i+\frac{1}{2}}^\top X_{i+\frac{1}{2}} \tilde{U}^\top U_{i+\frac{1}{2}}$$

Since $X_\dagger^\top X_\dagger = I$,

$$X_{i+1}^\top U_{i+1} = (X_\dagger^\top X_\dagger)^{-\frac{1}{2}} X_{i+\frac{1}{2}}^\top (U_{i+\frac{1}{2}} - \eta X_{i+\frac{1}{2}} \tilde{U}^\top U_{i+\frac{1}{2}}) = 0$$

So we proved all the constrain are satisfied again, which means $X_{i+1}^\top X_{i+1} = I$, $Y_{i+1}^\top + Y_{i+1} = 0$, $X_{i+1}^\top V_{i+1} = 0$, $p_{i+1} = p_{i+1}^\top$ \square

M Optimization on $\text{SO}(n)$ as a special case for $n = m$ on $\text{St}(n, m)$

Our method for Stiefel optimization can naturally be applied on the special orthogonal group $\text{SO}(n)$ (Appendix A.3) and is defined as follows

$$\text{SO}(n) := \{X \in \mathbb{R}^{n \times n} : X^\top X = I_n, \det X = 1\}. \quad (32)$$

[39] proposed an efficient algorithm based on Lie group structure for the optimization on $\text{SO}(n)$ although it cannot be generalized to Stiefel case. Our method restores the same integrator in [39] while using different approach applied to a family of metrics.

In greater detail, for $\text{SO}(n)$, the canonical-type metric (2) degenerates to Euclidean metric up to constant scaling, i.e., $g(\Delta_1, \Delta_2) = (1 - a)\text{Tr}(\Delta_1^\top \Delta_2)$. Then the corresponding Lagrangian is

$$L(X, \dot{X}, t) = r(t) \left[\frac{1-a}{2} \text{Tr}(\dot{X}^\top \dot{X}) - f(X) \right] - \frac{1}{2} \text{Tr}(\Lambda^\top (X^\top X - I)), \quad (33)$$

which results in the following position-momentum (X, Q) dynamics

$$\begin{cases} \dot{X}(t) = Q(t) \\ \dot{Q}(t) = -\gamma(t)Q(t) - X(t)Q(t)^\top Q(t) \\ \quad - \frac{\partial f}{\partial X}(t) + \frac{1+b}{2}X(t)X^\top(t) \frac{\partial f}{\partial X}(t) + \frac{1-b}{2}X(t) \frac{\partial f}{\partial X}(t)^\top X(t) \end{cases} \quad (34)$$

with the same initialization as (5). Next, apply the same Y, V decomposition of Q . Since $I - XX^\top = 0$, we have $V = 0$, i.e., the momentum Q is purely in Y -direction. Hence the equivalent dynamics to (34) is the following

$$\begin{cases} \dot{X}(t) = X(t)Y(t) \\ \dot{Y}(t) = -\gamma Y(t) - \frac{1-b}{2} \left(X^\top(t) \frac{\partial f}{\partial X}(t) - \frac{\partial f}{\partial X}^\top(t) X(t) \right). \end{cases} \quad (35)$$

Note when we take $b = -1$ (namely, $a = 1/2$), (35) is identical to the continuous dynamics in [39], although [39] uses an intrinsic form which is coordinate-free but not explicit enough.

The numerical integrator corresponding to (S)GD is defined the same as Section K.4 and is summarized in Alg.4. Note Step 5 is optional in the $n = m$ case. It gives the identity map if no arithmetic error due to machine precision is incurred. However, this step is beneficial under low precision (see Appendix K.1).

In addition, we also have an adaptive version which was absent in [39]:

Algorithm 4: Momentum SGD on $\text{SO}(n)$ (generalization to [39])

Hyperparameter: $\eta \in (0, +\infty)$, $\gamma \in [0, +\infty)$, $a < 1$, maximum number of iteration N

Initialization: X_0, V_0, Y_0 s.t. $X_0^\top X_0 = I$, $X_0^\top V_0 = 0$, $Y_0 + Y_0^\top = 0$, $b = \frac{a}{a-1}$

Output: Local minimum X of f

```

1 for  $i = 0, \dots, N - 1$  do
2    $f_i = \frac{1-b}{2} \left( X_i^\top \frac{\partial f}{\partial X}(X_i) - \frac{\partial f}{\partial X}(X_i)^\top X_i \right)$ 
3    $Y_{i+1} = \mu Y_i - f_i$ 
4    $X_{\dagger} = X_i \expm(\eta Y_{i+1})$ 
5    $X_{i+1} = X_{\dagger} (X_{\dagger}^\top X_{\dagger})^{-\frac{1}{2}}$ 
6 end
7 return  $X_N$ 

```

M.1 Adam on $\text{SO}(n)$

In this section, we extend the above optimizer to an Adam version. Note it can be derived from either the special case of the Stiefel optimizer, or the structure of Lie algebra $\mathfrak{so}(n)$, i.e., left-trivialization (see [39]) such that the momentum Y can be recognized as an element in $T_I \text{SO}(n)$, the tangent

space at the identity. In the latter interpretation, the momentum will always stay in the same tangent space $T_I \text{SO}(n)$ which passes on a message that trivialization almost reproduce the convenience in Euclidean space for $\text{SO}(n)$. Hence unlike the general Adam-Stiefel optimizer (Algo. 2), no extra technique, for example projection, is needed for Adam-SO(n). Detailed iterations are shown in Algo. 5. Note this is also a structure preserving scheme (see Thm. 9).

Algorithm 5: Adam on $\text{SO}(n)$

Hyperparameter : $\eta \in (0, +\infty)$, $\beta_1 \in [0, 1)$, $\beta_2 \in [0, 1)$, $0 < \epsilon \ll 1$, maximum number of iteration N

Initialization : X_0, V_0, Y_0 s.t. $X_0^\top X_0 = I$, $X_0^\top V_0 = 0$, $Y_0 + Y_0^\top = 0$, $p_0 = 0$, $q_0 = 0$

```

1 for  $i = 0, \dots, N - 1$  do
2    $f_i = \frac{1-b}{2} \left( X_i^\top \frac{\partial f}{\partial X}(X_i) - \frac{\partial f}{\partial X}(X_i)^\top X_i \right)$ 
3    $p_{i+1} = \beta_2 p_i + (1 - \beta_2) f_i^{\circ 2}$ 
4    $Y_{i+1} = \beta_1 Y_i - (1 - \beta_1) f_i$ 
5    $X_\dagger = X_i \text{expm} \left( \eta \sqrt{1 - \beta_2^{i+1}} Y_{i+1} \odot (p_{i+1}^{\circ -\frac{1}{2}} + \epsilon) \right)$ 
6    $X_{i+1} = X_\dagger (X_\dagger^\top X_\dagger)^{-\frac{1}{2}}$ 
7 end
8 return  $X_N$ 

```

Remark 5 (Details about Table 1: complexities and pros and cons of algorithms). In Table 1, the complexities are compared up to logarithmic terms for one iteration. For our method, the most costly operation is the $n \times m$ matrix multiplication (note $n > m$). The computation for the matrix exponential and square root of matrix inversion, is cautiously designed to only deal with matrices of dimension $m \times m$ (see Appendix K.1K.2), and thus admits at most $\mathcal{O}(m^3)$ at each step (particularly, forward Euler only has the complexity of $\mathcal{O}(m^2)$ while Cayley map takes $\mathcal{O}(m^3)$). For the inner loop of the square root of matrix inversion (Algo. 3), due to its quadratic convergence [53], it takes $\mathcal{O}(\log \log(1/\mathbf{u}))$ number of steps to achieve the machine precision \mathbf{u} . Note early stopping can be applied to this loop so that the complexity can be further reduced while the order of the overall method (1st-order) can still be maintained. The combination of all the above gives the complexity $\mathcal{O}(nm^2) + \mathcal{O}(m^3 \log \log(1/\mathbf{u}))$.

For other related methods, projected Stiefel SGD/Adam [7] includes the $n \times n$ matrices due to projection and retraction and therefore is much more expensive under the same order of accuracy as ours. Momentumless Stiefel (S)GD [38] shares the same complexity as our method but cannot be applied to other metrics or add momentum due to the failure of maintaining low rank structure that simplifies the computation. Regularizer methods have only $\mathcal{O}(nm^2)$ complexity per iteration but they cannot guarantee the variables to exactly stay on the manifold.

N Experimental details

Note: codes are provided in supplementary materials.

Experiments are conducted on a high-performance computing cluster whose name shall be revealed post anonymous period. Single v100 GPU was used.

N.1 General discussion

Initialization For variable X with the initial X_0 , in fact, any initialization with full rank is valid, including the non-orthogonal X_0 such that X_0 does not start on the manifold. This is due to the structure-preserving property of our algorithm (both SGD and Adam versions, see Appendix K). After just one iteration, X will stay on the manifold. Here we suggest one way of obtaining orthogonal X_0 which is performed in [4]. After randomly generating an entry-wise i.i.d. normal distributed n -by- m matrix, we can perform the QR decomposition. Denote the orthogonal matrix from QR decomposition as \tilde{Q} and denote the diagonal matrix which is the sign of the diagonal elements of R as \tilde{R} . Then we can take $X_0 = \tilde{Q}\tilde{R}$ and thus have $X_0^\top X_0 = I$.

For the variables U, Z in Stiefel SGD and U, Z, p, q in Stiefel Adam, we would use zero matrices as their initialization since zero matrices always satisfy these constraints (25).

No need to tune learning rate separately for constrained and unconstrained parameters For problems with both constrained and unconstrained parameters (Stiefel and Euclidean spaces), for example, the ViT test in Sec. 3, existing literatures using projection, retraction, and intermediate matrices (see Sec. 1.1) requires separate adjustments of learning rates for the two types of parameters. As an illustration, in projected SGD and Adam on Stiefel manifold [7], learning rate may vary 10s of times for constrained and unconstrained parameters. This can be intuitively understood as the result of applying different optimization methods for different parameters. However, using various learning rates may lead to the divergence of the algorithms.

In contrast, our Stiefel method can be established for both the constrained and unconstrained parameters with the same learning rate. Due to the same derivation of numerical methods for these two types, the effort in tuning hyperparameters is reduced while there is still good performance. In practice, the learning rate need to be adjusted in Stiefel SGD and momentum can be chosen as 0.9 for most machine learning tasks. For Stiefel Adam, we recommend to use 10^{-3} to be the learning rate and $(\beta_1, \beta_2) = (0.9, 0.999)$.

How to choose between Adam-Stiefel and momentum SGD-Stiefel Generally, we recommend choosing momentum SGD-Stiefel for traditional optimization and small scale neural networks that hyperparameters can be carefully adjusted while for large scale neural networks, use Adam-Stiefel as default.

N.2 Details of PRW

For MNIST experiment, we use a pretrained CNN to extract 128-dim. features of figures in MNIST. For Shakespeare’s plays experiment, we compute the PRW distances between all pairs of items in a corpus of eight Shakespeare’s operas embedded into 200-dim. space using word2vec. For each digit or play pair, we use the extracted features as point sets $\{x_i\}$ and $\{y_i\}$. We choose the dimension of the target space of the projection to be $k = 2$ in both experiments. The mean optimal transport values are taken among all digits or movie pairs at the specific iteration. All the setting are same as the original paper [3] except that early termination is removed.⁶

N.3 Details of ViT experiments

The structure of ViT and training process is exactly same as <https://github.com/omihub777/ViT-CIFAR> but we use a different ViT implementation from <https://github.com/lucidrains/vit-pytorch>. The hyperparameters are carefully adjusted for each optimizer to obtain the best performance. For projected Stiefel SGD/Adam [7], we tune the learning rates for constrained and unconstrained parameters separately. For regularizer SGD/Adam, the regularizer scaling parameter is also carefully chosen. The largest learning rate for momentumless Stiefel SGD [38] is applied but momentum methods still admit faster convergence. Additional experimental results can be seen in Fig. 2.

O Additional experiment: systematic tests on the leading eigenvalue problem

In this section, we consider the leading eigenvalue problem: given an n -by- n matrix A , find the m largest eigenvalues of A . This problem is at the core of many data sciences tasks, where n can be very large but m remains small. Due to its relative simplicity and the existence of exact solution, it’s possible to implement a large amount of experiments in order to systematically investigate the convergence, manifold perseverance, and time consumption of various approaches. Particularly, this problem can be formulated as an optimization problem on $\text{St}(n, m)$ as follows

$$\arg \max_{X \in \text{St}(n, m)} \text{Tr}(X^\top AX). \quad (36)$$

⁶Adam-type methods are not included since they are not suitable for this problem.

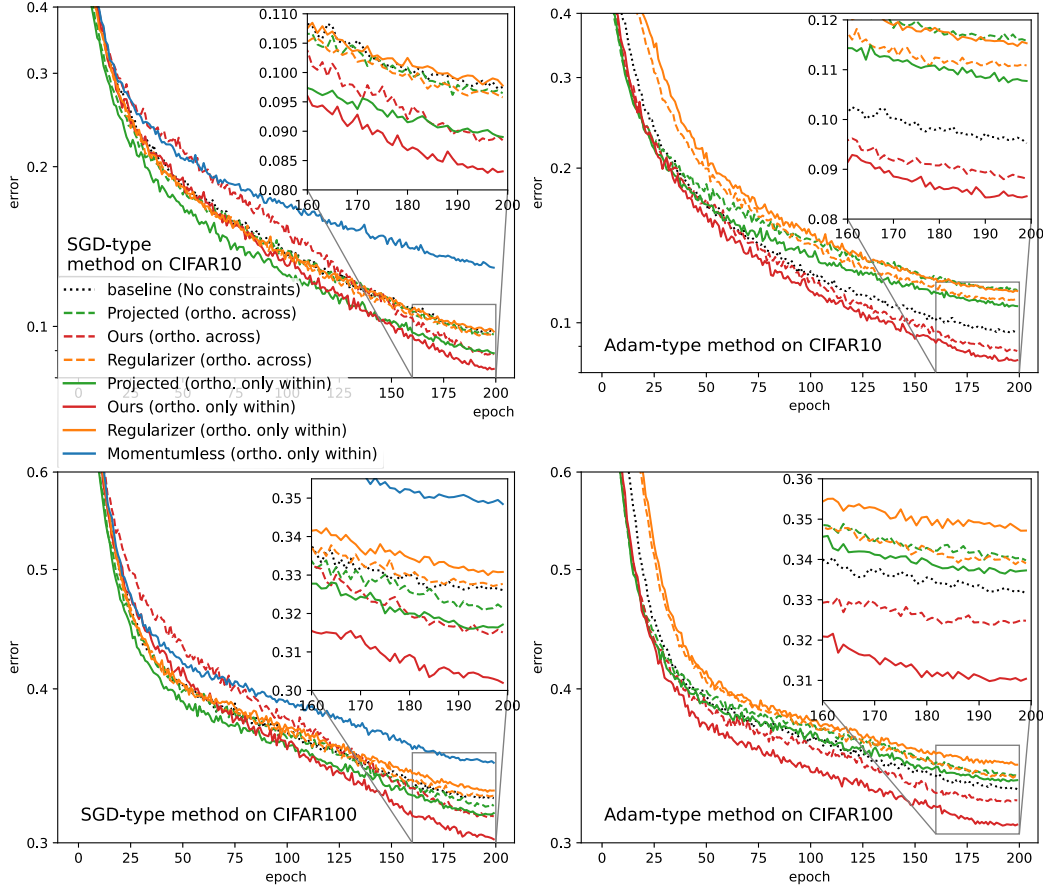


Figure 2: Test errors of Stiefel-ViT on CIFAR. We can see that our optimizer has the best test accuracy in both cases. Meanwhile, when our optimizer is used, orthogonality only within each head performs better than orthogonality across heads.

Such formulation is not unique. For example, [39] considers applying their momentum-accelerated $SO(n)$ optimizer to $\arg \min_{R \in SO(n)} \text{Tr}(E^T R^T A R E)$, where the constant padding matrix $E := [I_{m \times m}; 0_{(n-m) \times m}]$. However, their setting is computationally less efficient than our Stiefel simplification.

Our test uses a deterministic matrix A generated by $A = (\Xi + \Xi^T)/2/\sqrt{n}$, where Ξ is an instance of n -by- n matrix with i.i.d. random normal elements. The exact solution is obtainable from matrix decomposition so that the error can be quantified. As is mentioned above, several aspects of our algorithm are examined, including convergence speed, manifold perseverance, and computational complexity in Fig. 3, as well as other exact manifold-preserving methods. We can conclude that our (S)GD-Stiefel method has the fastest convergence rate and exact manifold perseverance with the lowest computational complexity.

Additionally, in Fig. 4, we test the influence of different canonical-type metric, i.e., different a in Def. 1, and the three different ways to ‘compute’ matrix exponential in Appendix K.2, i.e., the matrix exponential itself, Cayley map, and forward Euler. No significant difference is found in leading eigenvalue test and as a result, the most commonly used canonical metric and the cheapest forward Euler are chosen as default in all the other experiments.

⁷Only the time consumed by steps of optimizers is recorded but not time consumed by computing gradient

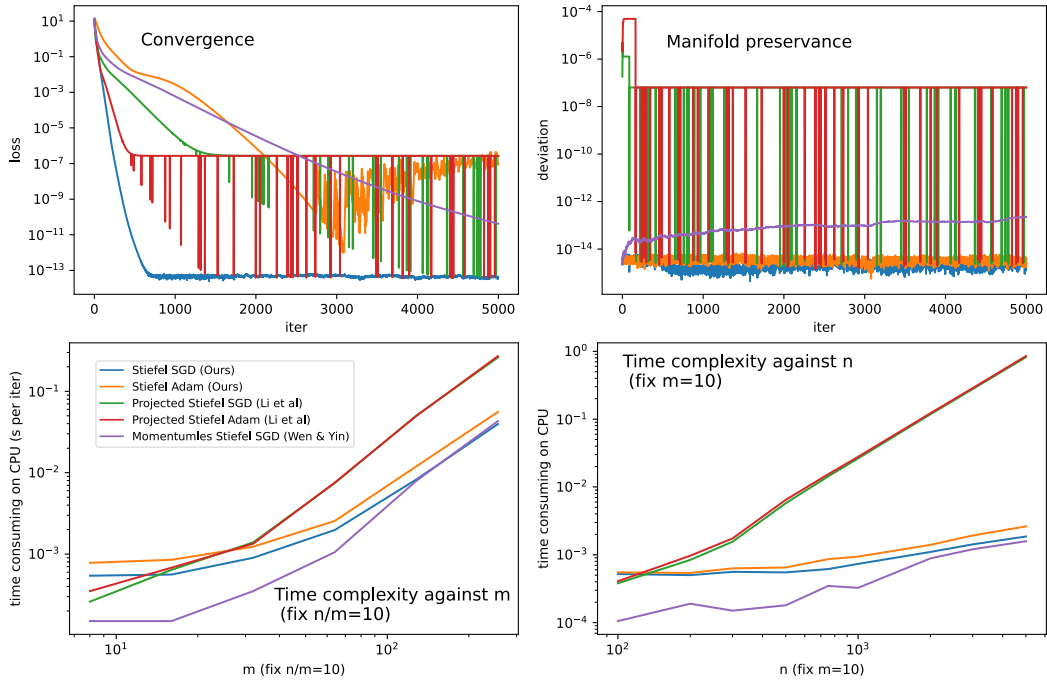


Figure 3: Comparison of exact manifold preserving methods on leading eigenvalue problem. The algorithms are performed on CPU with learning rate of each one adjusted to its best performance. The upper two figures show that our Stiefel SGD optimizer has the fastest convergence and best manifold perseverance. The lower two figures experimentally prove that we have the lowest $\mathcal{O}(nm^2)$ complexity per iteration, which matches our complexity analysis in Remark 5 and table 1⁷

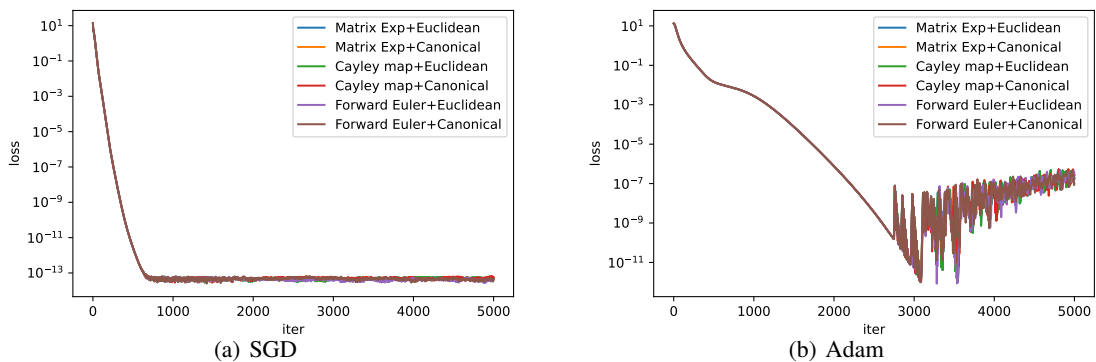


Figure 4: Comparison of different canonical-type metrics (Euclidean and canonical metrics are tested) and different ways to approximate matrix exponential in Appendix K.2.